ELSEVIER

Journal of Fluids and Structures 21 (2005) 665–687

JOURNAL OF FLUIDS AND STRUCTURES

www.elsevier.com/locate/jfs

Pipes conveying pulsating fluid near a 0 : 1 resonance: Global bifurcations

R.J. McDonald[a], N. Sri Namachchivaya[b,*]

[a]*Boeing Satellite Systems, Inc., El Segundo, CA 90245, USA*
[b]*Department of Aerospace Engineering, University of Illinois at Urbana–Champaign, Urbana, IL 61801, USA*

Received 28 July 2004; accepted 27 July 2005

Abstract

We study the global dynamics of parametrically excited pipes conveying fluid near a 0 : 1 resonance. A major goal of the analysis is to understand how energy may be transferred from the high-frequency mode to the low-frequency mode in these systems. We study the bifurcations of supported pipes conveying fluid, focusing on the subharmonic resonance case. Finally, using recently developed global bifurcation methods, we detect the presence of orbits which are homoclinic to certain invariant sets for the resonant case. In the dissipative case, we are able to identify conditions under which a generalized Šilnikov orbit would exist. In certain parameter regions, we prove that such orbits exist which are homoclinic to fixed points on the slow manifold, leading to chaotic dynamics in the system. These orbits provide the mechanism by which energy transfer between modes may occur.

1. Introduction

In this paper, we extend the study of McDonald and Namachchivaya (2005) on the dynamics of supported pipes conveying pulsating fluid to examine their global bifurcations close to a 0 : 1 resonance. The term *global bifurcation* refers to a qualitative change in the system dynamics that cannot be understood using local bifurcation theory. Examples of such phenomena include the creation of homoclinic or heteroclinic orbits, or the creation of new periodic orbits where no fixed point existed. Although global phenomena can sometimes be predicted from a local analysis [see, for example, the analysis of the double zero eigenvalue case in Guckenheimer and Holmes (1983)], local bifurcation methods are not sufficient to describe these bifurcations.

When the pipe oscillates, the flow of fluid through the pipe introduces a gyroscopic or Coriolis force which is proportional to the fluid velocity. For small flow velocities, there is little coupling between the fluid and the structure. Centrifugal forces in the pipe act in much the same way as compressive forces do in a beam. Hence, increasing the fluid velocity decreases the effective stiffness of the pipe system, and may lead to buckling, also known as divergence. In the absence of damping, the Coriolis forces act to re-stabilize the pipe after divergence before flutter finally destabilizes the pipe. For an undamped system with no external tension or gravity, the classical result is that divergence of the first mode occurs at a dimensionless critical velocity of $u_c = \pi$.

*Corresponding author. Tel.: +1 217 333 2651; fax: +1 217 244 0720.
E-mail address: navam@uiuc.edu (N. Sri Namachchivaya).

0889-9746/$ - see front matter © 2005 Published by Elsevier Ltd.
doi:10.1016/j.jfluidstructs.2005.07.015

In this paper, we study the global bifurcations of simply supported damped pipe systems *near the critical velocity* u_c, when the fluid velocity is also pulsating. The goal of our analysis will be to understand the effect that the forcing and damping has on this gyroscopic system in the neighborhood of the 0 : 1 critical point. In many dynamical systems with homoclinic or heteroclinic orbits between fixed points, chaotic dynamics may be present. Several global bifurcation methods may be used to detect chaos in systems that possess homoclinic/heteroclinic orbits. One method, due to Melnikov (1963), and described in Guckenheimer and Holmes (1983) and Wiggins (1988), provides conditions under which a homoclinic orbit to a saddle node in the unperturbed system may break under perturbation, allowing the stable and unstable manifolds of the saddle node to intersect transversally. Such intersections may lead to global bifurcations and chaos in the system. A second method, described by Kovačič and Wiggins (1992), determines conditions under which a Šilnikov-type homoclinic orbit may be present in a perturbed resonant system. These Šilnikov orbits have two time scales, spending a long time near a slow manifold before making a fast pulse and returning to the same slow manifold or another slow manifold. Šilnikov (1965) showed that perturbation of these orbits might lead to chaotic dynamics in the system. A third method, due to Haller and Wiggins (1995) detects similar Šilnikov-type orbits which made several quick pulses away from the slow manifold. Šilnikov's result can also be applied to these generalized Šilnikov orbits, giving another tool for the detection of chaos in the system. We will investigate the possibility of chaotic dynamics in these systems using these methods.

Since the latter two of these methods involve an exchange of energy between the modes of a system, these methods may be useful in describing the energy transfer that we expect to occur between the two resonant modes in our problem. The primary method we use is the method to detect multi-pulse homoclinic orbits, and we apply this method to the system forced at subharmonic resonance. We first determine conditions under which the system possesses multi-pulse orbits that are homoclinic to a slow manifold in the system. We then determine parameter regions where the damped system has orbits which are homoclinic to a saddle focus fixed point. The presence of such homoclinic orbits leads to chaotic behavior in the system through Smale horseshoes. Finally, we try to give some physical interpretations to these global phenomena for the physical systems considered.

There have been many applications of the Šilnikov and multi-pulse methods to study the global dynamics of engineering systems, and we mention a few here. The first application of the Šilnikov method was in the study of the nonlinear Schrödinger (NLS) equations by Kovačič and Wiggins (1992). Feng and Sethna (1993) found single pulse Šilnikov orbits for thin parametrically excited plates. Tien et al. (1994a, b), and Malhotra and Namachchivaya (1995) found single pulse Šilnikov orbits for the forced motion of shallow arches and suspended elastic cables. Kovačič and Wettergren (1996) found single and multi-pulse methods in resonantly driven coupled pendula. The first application of the multi-pulse method was by Haller and Wiggins (1995) to study the NLS equations. Haller (1998, 1999) gives several example problems using this method, including a forced beam, resonant surface wave interactions, and a nonlinear vibration absorber. Malhotra and Namachchivaya (1995) located single and multi-pulse orbits in the transverse motion of a spinning disk, using both the Šilnikov and multi-pulse techniques.

In Section 2, we present the equations of motion in the Hamiltonian form as in McDonald and Namachchivaya (2005) and the normal form for the pipe system near the critical point at which the system possesses a nonsemisimple double zero eigenvalue. In Section 3, we focus on the subharmonic resonance case, since the global bifurcation methods we use are not applicable to the combination resonance case. The geometric structure of the unperturbed integrable Hamiltonian problem is used to develop an appropriate set of *coordinates* for studying the perturbed problem. After obtaining detailed information on the nature of the unperturbed system, in Section 4 we use three methods called the *Melnikov method*, the *Šilnikov method*, and the *multi-pulse method* to detect the presence of chaotic dynamics in the system studied. Finally in Section 5, we summarize the results and interpret them in terms of the physical motion of pipe conveying pulsating fluid.

2. Formulation

We shall first briefly derive the ODEs for the parametrically excited pipe system. We include the effects of nonlinearities and damping, as well as a time-dependent fluid velocity. The Hamiltonian equations of motion are given by McDonald and Namachchivaya (2005):

$$\dot{\mathbf{x}} = A\mathbf{x} + JDH_1(\mathbf{x}) + \varepsilon\{h(\dot{f}(t)D_s + f(t)D_c - \zeta^* D_d)\}\mathbf{x} - \varepsilon\zeta^* F(\mathbf{x}), \tag{1}$$

where $\mathbf{x} = [q_1\ q_2\ p_1\ p_2]^{\mathrm{T}}$, and

$$A = \begin{bmatrix} 0 & \frac{8}{3}M_r u_0 & 1 & 0 \\ -\frac{8}{3}M_r u_0 & 0 & 0 & 1 \\ -\bar{\omega}_1^2 & 0 & 0 & \frac{8}{3}M_r u_0 \\ 0 & -\bar{\omega}_2^2 & -\frac{8}{3}M_r u_0 & 0 \end{bmatrix}, \tag{2}$$

$$F(\mathbf{x}) = \begin{bmatrix} 0 \\ 0 \\ f_1(\mathbf{q},\mathbf{p}) \\ f_2(\mathbf{q},\mathbf{p}) \end{bmatrix} = \begin{bmatrix} 0 \\ 0 \\ 2\kappa\pi^2\left(\pi^2 q_1\left(p_1 + \frac{8}{3}M_r u_0 q_2\right) + 4\pi^2 q_2\left(p_2 - \frac{8}{3}M_r u_0 q_1\right)\right)q_1 \\ 8\kappa\pi^2\left(\pi^2 q_1\left(p_1 + \frac{8}{3}M_r u_0 q_2\right) + 4\pi^2 q_2\left(p_2 - \frac{8}{3}M_r u_0 q_1\right)\right)q_2 \end{bmatrix}, \tag{3}$$

$$D_s = \begin{bmatrix} 0 & 0 \\ -D_{1,s} & 0 \end{bmatrix}, \quad D_c = \begin{bmatrix} 0 & 0 \\ -D_{1,c} + D_{2,c}G & -D_{2,c} \end{bmatrix}, \tag{4}$$

$\Lambda = \mathrm{diagonal}\{\lambda_1^4, \lambda_2^4\} = \{\pi^4, 16\pi^4\}$ and

$$D_d = \begin{bmatrix} 0 & 0 \\ \Lambda G & \Lambda \end{bmatrix}, \quad D_{1,s} = M_r u_0 \begin{bmatrix} -\frac{\pi^2}{2} & -\frac{64}{9} \\ -\frac{16}{9} & -2\pi^2 \end{bmatrix}, \quad D_{1,c} = 2u_0 \begin{bmatrix} -\pi^2 & 0 \\ 0 & -4\pi^2 \end{bmatrix}. \tag{5}$$

We specify the form of the forcing as $f(t) = \cos \nu t$ and the nonlinear Hamiltonian term $H_1(\mathbf{q},\mathbf{p})$ is given by

$$H_1(\mathbf{q},\mathbf{p}) = \frac{\kappa\pi^4}{4}(q_1^2 + 4q_2^2)^2, \tag{6}$$

and the two quantities $\bar{\omega}_1$ and $\bar{\omega}_2$ are defined as

$$\bar{\omega}_1^2 = \pi^2(\pi^2 - (u_0^2 - \bar{T})) + \tfrac{64}{9}M_r^2 u_0^2 = \omega_1^2 + g_{21}^2,$$
$$\bar{\omega}_2^2 = 4\pi^2(4\pi^2 - (u_0^2 - \bar{T})) + \tfrac{64}{9}M_r^2 u_0^2 = \omega_2^2 + g_{21}^2.$$

Eq. (1) represents the equations of motion (Hamiltonian form) for a two-mode truncation of the pipe conveying fluid.

The eigenvalues of A are

$$\pm\mathrm{i}\sqrt{\tfrac{64}{9}M_r^2 u_0^2 + \tfrac{1}{2}(\bar{\omega}_1^2 + \bar{\omega}_2^2) \mp \sqrt{\tfrac{128}{9}M_r^2 u_0^2(\bar{\omega}_1^2 + \bar{\omega}_2^2) + \tfrac{1}{4}(\bar{\omega}_1^2 - \bar{\omega}_2^2)^2}}.$$

We wish to study the system when it possesses a pair of zero eigenvalues. For simplicity, we will describe this motion for $\bar{T} = 0$. For $u_0 = 0$, the eigenvalues are at $\{\pm\mathrm{i}\pi^2, \pm 4\mathrm{i}\pi^2\}$. As u_0 is increased, both pairs of eigenvalues move towards the origin along the imaginary axis, until $u_0 = \pi$, when the eigenvalues from the first mode become zero. These eigenvalues split, and move onto the real axis. Eventually, this first mode pair of eigenvalues reverses its direction, and moves back towards the origin. What happens next depends on the value of M_r. If $M_r < (3\sqrt{3}/32)\pi$, then the eigenvalues from the second mode reach zero at $u_0 = 2\pi$, split, and move onto the real axis. These eigenvalues eventually coalesce along the real axis, and leave that axis. For $M_r > (3\sqrt{3}/32)\pi$, the eigenvalues from the first mode reach zero first at $u_0 = 2\pi$, re-stabilizing that mode. The two pairs of eigenvalues eventually coalesce along the imaginary axis, and split, indicating the onset of flutter. These two cases are shown in McDonald and Namachchivaya (2005).

Thus, there are two critical flow velocities at which the system has a double zero eigenvalue, $u_0 = \pi$ and 2π. If tension is present in the system, the corresponding critical flow velocities are $u_0 = (\pi^2 + \bar{T})^{1/2}$ and $u_0 = (4\pi^2 + \bar{T})^{1/2}$. A key idea here is to calculate the normal form for the system at these critical flow velocities. The normal form near $u_0 = u_0^c$ was derived in McDonald and Namachchivaya (2005) using the methods developed in McDonald et al. (1999)

and is given as

$$\dot{w}_1 = -\frac{\mathrm{i}}{2}(w_1-\bar{w}_1)+\frac{\mathrm{i}\beta_1\delta}{2}(w_1+\bar{w}_1)+4\mathrm{i}\alpha_1(w_1+\bar{w}_1)^3+2\mathrm{i}\alpha_2(w_1+\bar{w}_1)w_2\bar{w}_2+\zeta^*\delta_1 w_1+\sigma_1 w_2-\bar{\sigma}_1\bar{w}_2 + \zeta^*[\phi_1 w_1 w_2\bar{w}_2+\phi_2 w_1(w_1+\bar{w}_1)^2+\phi_3(w_1+\bar{w}_1)w_2\bar{w}_2+\phi_4(w_1+\bar{w}_1)^3],$$

$$\dot{w}_2 = -\mathrm{i}\lambda\Lambda_1 w_2+\mathrm{i}\beta_2\delta w_2+\mathrm{i}\alpha_2(w_1+\bar{w}_1)^2 w_2+2\mathrm{i}\alpha_3 w_2^2\bar{w}_2 + \zeta^*\delta_2 w_2-\bar{\sigma}_1(w_1+\bar{w}_1)+\sigma_4\bar{w}_2+\zeta^*[\phi_5 w_2^2\bar{w}_2+\phi_6(w_1+\bar{w}_1)^2 w_2], \tag{7}$$

where the coefficients in terms of the original coefficients are given in McDonald and Namachchivaya (2005). We note that the equations for the two cases (subharmonic and combination resonances) are now identical, except for the forcing terms. The unperturbed Hamiltonian is given by

$$H=\frac{\mathrm{i}}{4}(w_1-\bar{w}_1)^2+\frac{\mathrm{i}\beta_1\delta}{4}(w_1+\bar{w}_1)^2-\mathrm{i}\Lambda_1(1+\lambda)w_2\bar{w}_2+\mathrm{i}\beta_2\delta w_2\bar{w}_2 + \mathrm{i}\alpha_1(w_1+\bar{w}_1)^4+\mathrm{i}\alpha_2(w_1+\bar{w}_1)^2 w_2\bar{w}_2+\mathrm{i}\alpha_3 w_2^2\bar{w}_2^2.$$

The geometric structure of the unperturbed integrable Hamiltonian problem is used to develop an appropriate set of *coordinates* for studying the perturbed problem. The fast motions (Hamiltonian) in (7) can be effected by appropriately introducing a set of new co-ordinates having cyclic character, if such can be found. To this end, it is convenient to transform the equations of motion to action-angle form, using the transformation

$$w_1=\sqrt{2I_1}\mathrm{e}^{\mathrm{i}\theta_1},\quad w_2=\sqrt{2I_2}\mathrm{e}^{\mathrm{i}\theta_2}$$

This transformation is symplectic with multiplier 2i. For both cases, the unperturbed Hamiltonian in action-angle coordinates is given by

$$H(\theta_1,\theta_2,I_1,I_2)=\frac{1}{2\mathrm{i}}H(z_1(\theta,I),z_2(\theta,I)) = -I_1\sin^2\theta_1+\beta_1\delta I_1\cos^2\theta_1+(\beta\delta_2-\lambda\Lambda_1)I_2+32\alpha_1 I_1^2\cos^4\theta_1+8\alpha_2 I_1 I_2\cos^2\theta_1+2\alpha_3 I_2^2.$$

For the combination resonance case, we obtain the equations

$$\begin{aligned}
\dot{\theta}_1 &= -\sin^2\theta_1+\beta_1\delta\cos^2\theta_1+64\alpha_1 I_1\cos^4\theta_1+8\alpha_2 I_2\cos^2\theta_1 \\
&\quad +2\sqrt{\frac{I_2}{I_1}}\cos\theta_1(\sigma_1^r\sin\theta_2+\sigma_i^i\cos\theta_2)+\zeta^*[4\phi_3^i I_2\cos^2\theta_1+16\phi_4^i I_1\cos^4\theta_1], \\
\dot{\theta}_2 &= \beta_2\delta-\lambda\Lambda_1+8\alpha_2 I_1\cos^2\theta_1+4\alpha_3 I_2-2\sqrt{\frac{I_1}{I_2}}\cos\theta_1(-\sigma_1^r\sin\theta_2-\sigma_1^i\cos\theta_2)+8\zeta^*\phi_6^i I_1\cos^2\theta_1, \\
\dot{I}_1 &= 2(1+\beta_1\delta)I_1\cos\theta_1\sin\theta_1+128\alpha_1 I_1^2\cos^3\theta_1\sin\theta_1+16 I_1 I_2\cos\theta_1\sin\theta_1 \\
&\quad +4\sqrt{I_1 I_2}\sin\theta_1(\sigma_1^r\sin\theta_2+\sigma_1^i\cos\theta_2)+2\zeta^*\delta_1 I_1+\zeta^*[4\phi_1 I_1 I_2+16\phi_2 I_1^2\cos^2\theta_1 \\
&\quad +8\phi_3^i I_1 I_2\cos\theta_1\sin\theta_1+32\phi_4^i I_1^2\cos^3\theta_1\sin\theta_1], \\
\dot{I}_2 &= 2\zeta^*\delta_2 I_2+4\sqrt{I_1 I_2}\cos\theta_1(-\sigma_1^r\cos\theta_2+\sigma_1^i\sin\theta_2)+\zeta^*[4\phi_5 I_2^2+16\phi_6^r I_1 I_2\cos^2\theta_1];
\end{aligned} \tag{8}$$

and for the subharmonic resonance, we obtain the equations

$$\begin{aligned}
\dot{\theta}_1 &= -\sin^2\theta_1+\beta_1\delta\cos^2\theta_1+64\alpha_1 I_1\cos^4\theta_1+8\alpha_2 I_2\cos^2\theta_1+\zeta^*[4\phi_3^i I_2\cos^2\theta_1+16\phi_4^i I_1\cos^4\theta_1], \\
\dot{\theta}_2 &= \beta_2\delta-\lambda\Lambda_1+8\alpha_2 I_1\cos^2\theta_1+4\alpha_3 I_2+\sigma_4^i\cos 2\theta_2-\sigma_4^r\sin\theta_2+8\zeta^*\phi_6^i I_1\cos^2\theta_1, \\
\dot{I}_1 &= 2(1+\beta_1\delta)I_1\cos\theta_1\sin\theta_1+128\alpha_1 I_1^2\cos^3\theta_1\sin\theta_1+16 I_1 I_2\cos\theta_1\sin\theta_1 \\
&\quad +2\zeta^*\delta_1 I_1+\zeta^*[4\phi_1 I_1 I_2+16\phi_2 I_1^2\cos^2\theta_1+8\phi_3 I_1 I_2\cos\theta_1\sin\theta_1+32\phi_4 I_1^2\cos^3\theta_1\sin\theta_1], \\
\dot{I}_2 &= 2\zeta^*\delta_2 I_2+2\sigma_4^r I_2\cos 2\theta_2+2\sigma_4^i I_2\sin\theta_2+\zeta^*[4\phi_5 I_2^2+16\phi_6^r I_1 I_2\cos^2\theta_1].
\end{aligned} \tag{9}$$

The generalized coordinates are (θ_1,θ_2), with corresponding generalized momenta (I_1,I_2).

3. Equations in standard form: subharmonic resonance case

The goal of our analysis will be to understand the effect that the forcing and damping has on this gyroscopic system in the neighborhood of the 0 : 1 critical point. We focus on the subharmonic resonance case, since the global bifurcation methods we will use in Section 4 are not applicable to the combination resonance case.

We now transform the equations of the first mode into a rectangular coordinate system in (9) to avoid singularities associated with $I_1 = 0$. We make the transformation

$$x = \sqrt{2I_1}\,\sin\,\theta_1, \quad y = \sqrt{2I_1}\,\cos\,\theta_1, \quad I = I_2, \quad \theta = \theta_2.$$

Hence, the equations that we need are given in coordinates (x, y, ϕ, I) in the form

$$\begin{aligned}
\dot{x} &= \beta_1\delta y + 32\alpha_1 y^3 + 8\alpha_2 Iy + \varepsilon\{\zeta\delta_1 x + \zeta[2\phi_1 Ix + 4\phi_2 xy^2 + 4\phi_3 Iy + 8\phi_4 y^3]\},\\
\dot{y} &= x + \varepsilon\{\zeta\delta_1 y + \zeta[2\phi_1 Iy + 4\phi_2 y^3]\},\\
\dot{I} &= \varepsilon\{2\zeta\delta_2 I + 2I\sigma_4 \sin 2\phi + \zeta[4\phi_5 I^2 + 8\phi_6^r Iy^2]\},\\
\dot{\phi} &= \beta_2\delta - \lambda\Lambda_1 + 4\alpha_2 y^2 + 4\alpha_3 I + \varepsilon\{\sigma_4\,\cos\,2\phi + 4\zeta^*\phi_6^i y^2\},
\end{aligned} \tag{10}$$

where we have also made the substitutions

$$\sigma_4^i\,\cos\,2\theta_2 - \sigma_4^r\,\sin\,2\theta_2 = \sigma_4\,\cos\,2\phi$$

with

$$\phi = \theta - \frac{D_s}{2}, \quad \sigma_4 = \sqrt{(\sigma_4^r)^2 + (\sigma_4^i)^2}, \quad \cos\,D_s = \frac{\sigma_4^i}{\sigma_4}.$$

These equations have the standard form

$$\begin{aligned}
\dot{\mathbf{x}} &= JD_{\mathbf{x}}H_0(\mathbf{x}, I) + \varepsilon\{JD_{\mathbf{x}}H_1(\mathbf{x}, I, \phi; \varepsilon) + f^{\mathbf{x}}(\mathbf{x}, I, \phi; \varepsilon)\},\\
\dot{I} &= \varepsilon\{-D_\phi H_1(\mathbf{x}, I, \phi; \varepsilon) + f^I(\mathbf{x}, I, \phi; \varepsilon)\},\\
\dot{\phi} &= D_I H_0(\mathbf{x}, I) + \varepsilon\{D_I H_1(\mathbf{x}, I, \phi; \varepsilon) + f^\phi(\mathbf{x}, I, \phi; \varepsilon)\},
\end{aligned} \tag{11}$$

where $\mathbf{x} = [x\ y]^{\mathrm{T}} \in \mathbb{R}^2$, $I \in \mathbb{R}$, $\theta \in \mathbb{S}^1$. The unperturbed Hamiltonian H_0 and perturbed Hamiltonian H_1 in these hybrid coordinates for this system are given by

$$\begin{aligned}
H_0 &= -\tfrac{1}{2}x^2 + \tfrac{1}{2}\beta_1\delta y^2 + (\beta_2\delta - \lambda\Lambda_1)I + 8\alpha_1 y^4 + 4\alpha_2 Iy^2 + 2\alpha_3 I^2,\\
H_1 &= \sigma_4 I\,\cos\,2\phi,
\end{aligned}$$

and the dissipative perturbations are given by

$$\begin{aligned}
f^{\mathbf{x}} &= \begin{bmatrix} \zeta\delta_1 x + 2\zeta\phi_1 Ix + 4\zeta\phi_2 xy^2 + 4\zeta\phi_3^i Iy + 8\zeta\phi_4^i y^3 \\ \zeta\delta_1 y + 2\zeta\phi_1 Iy + 4\zeta\phi_2 y^3 \end{bmatrix},\\
f^I &= 2\zeta\delta_2 I + 4\zeta\phi_5 I^2 + 8\zeta\phi_6^r Iy^2,\\
f^\phi &= 4\zeta\phi_6^i y^2.
\end{aligned}$$

The perturbation terms include the effects of both Hamiltonian and non-Hamiltonian perturbations. These perturbation terms (dissipative and forcing) can be written in more compact form as

$$g^{\mathbf{x}} = JD_{\mathbf{x}}H_1 + f^{\mathbf{x}}, \quad g^I = -D_\phi H_1 + f^I, \quad g^\phi = D_I H_1 + f^\phi.$$

3.1. Unperturbed dynamics

We note immediately that the unperturbed system, obtained by letting $\varepsilon \to 0$, is integrable, since it possesses two constants, the unperturbed Hamiltonian H_0 and the action coordinate I. We shall make a series of investigations about the unperturbed system.

3.1.1. Dynamics in x–y plane

First, we discuss the dynamics in the x–y plane for a given value of I. These dynamics are described by the equations

$$\dot{x} = \beta_1\delta y + 32\alpha_1 y^3 + 8\alpha_2 I y, \quad \dot{y} = x.$$

For the unperturbed Hamiltonian system in the four-dimensional phase space, we have $\dot{I} = 0$, so that I is a constant of the system. We can therefore define a constant function, $H^R(x, y, I)$ by

$$H^R(x, y, I) = -\frac{1}{2}x^2 + \frac{\beta_1\delta}{2}y^2 + 8\alpha_1 y^4 + 4\alpha_2 y^2 I.$$

In the x–y plane, we see that there is a trivial fixed point, denoted E_0 at $(x, y) = (0, 0)$. To study the stability of this fixed point, we first determine the eigenvalues of E_0, which are given by

$$\lambda_{1,2}^{E_0} = \pm\sqrt{\beta_1\delta + 8\alpha_2 I}.$$

Thus, E_0 is stable (imaginary eigenvalues) for $\beta_1\delta < -8\alpha_2 I$, while the system is unstable (real eigenvalues) for $\beta_1\delta > -8\alpha_2 I$. Since $\beta_1 > 0$ and $\alpha_2 < 0$, we have the following stability conditions for E_0:

$$E_0 \text{ stable:} \quad \delta < \frac{8|\alpha_2|I}{\beta_1};$$

or, in terms of I,

$$E_0 \text{ stable:} \quad I > \frac{\beta_1\delta}{8|\alpha_2|}.$$

The stability of E_0 changes at $\delta = 8|\alpha_2|I/\beta_1 > 0$. In terms of I, the stability changes at $I = \beta_1\delta/(8|\alpha_2|)$ which is positive if $\delta > 0$. However, if $\delta < 0$, the stability of E_0 does not change for a positive value of I, in which case the trivial fixed point E_0 does not bifurcate.

The system has another set of fixed points, denoted $E_1^{\pm}$, and given by

$$E_1^+ = (0, y_0), \quad E_1^- = (0, -y_0),$$

where

$$y_0 = \sqrt{\frac{\beta_1\delta + 8\alpha_2 I}{32|\alpha_1|}}.$$

These fixed points $E_1^{\pm}$only exist for $(\beta_1\delta + 8\alpha_2 I)/(32|\alpha_1|) > 0$, or $\beta_1\delta + 8\alpha_2 I > 0$. Thus, we have the following existence criteria for $E_1^{\pm}$:

$$E_1^{\pm} \text{ exists:} \quad \delta > \frac{8|\alpha_2|I}{\beta_1};$$

and in terms of I,

$$E_1^{\pm} \text{ exists:} \quad I < \frac{\beta_1\delta}{8|\alpha_2|}.$$

Comparing these with the stability conditions for E_0, we see that $E_1^{\pm}$ only exist when E_0 is unstable. We again check the stability of these fixed points by calculating eigenvalues at the fixed points $E_1^{\pm}$:

$$\lambda_{1,2}^{E_{1,2}} = \pm i\sqrt{2(\beta_1\delta + 8\alpha_2 I_2)}.$$

So $E_1^{\pm}$ are stable if $\beta_1\delta + 8\alpha_2 I_2 > 0$. The stability criteria for $E_1^{\pm}$ are then

$$E_1^{\pm} \text{ stable:} \quad \delta > \frac{8|\alpha_2|I}{\beta_1};$$

and in terms of I,

$$E_1^{\pm} \text{ stable:} \quad I < \frac{\beta_1\delta}{8|\alpha_2|}.$$

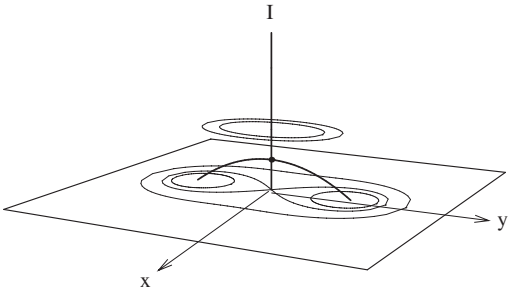

Fig. 1. Phase portrait for case $\delta>0$, $0<I<\frac{\beta_1\delta}{8|\alpha_2|}$.

Thus, we see that $E_1^{\pm}$, when they exist, are unstable, and have the opposite stability as E_0. Thus, depending on the sign of δ, the following two phase portraits are possible:

(i) $\delta<0$: E_0 is stable for $I>0$. Fixed points $E_1^{\pm}$ *do not exist*. Thus, for all $I>0$, the phase portrait simply consists of periodic orbits centered at E_0.
(ii) $\delta>0$: E_0 is unstable for $0<I<\beta_1\delta/(8|\alpha_2|)$ and stable for $I>\beta_1\delta/(8|\alpha_2|)$. Two branches of fixed points, $E_1^{\pm}$ exist for $0<I<\beta_1\delta/(8|\alpha_2|)$. These two branches bifurcate from E_0 at $I=\beta_1\delta/(8|\alpha_2|)$ and the bifurcating branches open downwards. Thus, there are two possible planar phase portraits, depending on the value of I:

  (a) $0<I<\beta_1\delta/(8|\alpha_2|)$: The unstable saddle point E_0 is connected to itself by a pair of homoclinic orbits, each of which encircles one of the stable centers $E_1^{\pm}$. These centers $E_1^{\pm}$ are surrounded by a continuous family of periodic orbits extending to the homoclinic orbit. Surrounding both homoclinic orbits is a continuous family of larger periodic orbits. The phase portrait for this case is given in Fig. 1.
  (b) $I>\beta_1\delta/(8|\alpha_2|)$: The phase portrait simply consists of a continuous family of periodic orbits centered around the stable center E_0.

A richer variety of phase portraits and orbit behavior is possible if we do not restrict the coefficients $\alpha_i<0$. However, since this restriction is present in the physical example considered, we only consider this case. The condition for homoclinic behavior to be present, $\delta>0$, corresponds to the bifurcation parameter (flow velocity) being *above* the critical value of that parameter.

Hence, the system (11) has a saddle fixed point, denoted by $\tilde{\mathbf{x}}_0(I)\stackrel{\text{def}}{=}(0,0)$. More precisely, for each value of I in some range $I\in(I_a,I_b)$, the two-dimensional system on the $\mathbf{x}$-plane has a saddle fixed point. In the four-dimensional phase space (i.e. including the I and θ coordinates), these fixed points extend to a two-dimensional normally hyperbolic manifold Π_0, defined by

$$\Pi_0=\{(\mathbf{x},I,\phi)|\mathbf{x}=\tilde{\mathbf{x}}_0(I),\ I_a<I<I_b, 0\leqslant\phi<2\pi\}=\{(x,y,I,\phi)|x=y=0\}.$$

3.1.2. Homoclinic orbits

For each value of $I\in(I_a,I_b)$, the system (11) has a homoclinic orbit, $\mathbf{x}^h(t,I)$, connecting the saddle fixed point to itself. In the four-dimensional phase space, these homoclinic orbits extend to a three-dimensional homoclinic manifold, defined by

$$\Gamma=\{(\mathbf{x},I,\theta)|\,\mathbf{x}=\mathbf{x}^h(t,I),\ I_a<I<I_b,\ \theta^h(t,I,\theta_0)\}.$$

This manifold contains the stable and unstable manifolds of the invariant manifold Π_0. These manifolds intersect nontransversally to form the homoclinic manifold.

We next determine the homoclinic orbits in the x–y plane. The homoclinic orbits only appear for the cases where $\alpha_1<0$. The Hamiltonian function H_0 will be constant on the homoclinic orbit, as will the coordinate I. We therefore define a constant function

$$H^R(x,y,I)=-\tfrac{1}{2}x^2+\tfrac{1}{2}\beta_1\delta y^2+8\alpha_1y^4+4\alpha_2Iy^2.$$

Essentially, we have just subtracted the constant terms from the unperturbed Hamiltonian in order to obtain a simpler constant function H^R. We note that since $(0,0)$ is on the orbit and $H^R(0,0)=0$, that $H^R=0$ on the entire homoclinic

orbit. This observation gives us a constant with which we may solve for the homoclinic orbit in the x–y plane. We therefore solve the equation

$$H^R(0,0) = H^R(x^h(t), y^{h(t)}),$$

where $(x^{h(t)}, y^{h(t)})$ is a time-parametrized expression for the homoclinic orbit. We obtain

$$0 = -\frac{1}{2}x^2 + \frac{\beta_1\delta}{2}y^2 + 8\alpha_1 y^4 + 4\alpha_2 y^2 I_2.$$

Solving this equation for x, and substituting this into the equation for $\dot{y}$ yields

$$\dot{y} = +y\sqrt{ay^2+b} \quad \text{for first and third quadrants;}$$
$$\dot{y} = -y\sqrt{ay^2+b} \quad \text{for second and fourth quadrants.}$$

The time-parameterized expressions for these orbits (in each of the four quadrants) are obtained from the above differential equations as

$$y_1^h(t) = \sqrt{-\frac{b}{a}}\operatorname{sech}\sqrt{b}t, \quad x_1^h(t) = y_1^h(t)\sqrt{ay_1^h(t)+b}, \quad -\infty < t < 0,$$
$$y_2^h(t) = \sqrt{-\frac{b}{a}}\operatorname{sech}\sqrt{b}t, \quad x_2^h(t) = -y_2^h(t)\sqrt{ay_2^h(t)+b}, \quad 0 < t < \infty,$$
$$y_3^h(t) = -\sqrt{-\frac{b}{a}}\operatorname{sech}\sqrt{b}t, \quad x_3^h(t) = y_3^h(t)\sqrt{ay_3^h(t)+b}, \quad -\infty < t < 0,$$
$$y_4^h(t) = \sqrt{-\frac{b}{a}}\operatorname{sech}\sqrt{b}t, \quad x_4^h(t) = -y_4^h(t)\sqrt{ay_4^h(t)+b}, \quad 0 < t < \infty,$$

where the coefficients (a, b) are defined by

$$a = 16\alpha_1 < 0, \quad b = 8\alpha_2 I + \beta_1\delta. \tag{12}$$

These orbits only exist if E_0 is unstable, i.e. $\beta_1\delta + 8\alpha_2 I > 0$.

We also need to solve for $\phi^h(t)$, as it will be required in later calculations. We have

$$\dot{\theta} = (\beta_2\delta - \lambda\Lambda_1 + 4\alpha_3 I) + 4\alpha_2 y^2 = \omega_A + 4\alpha_2 y^2,$$

where the first three terms on the right-hand side of this equation are constant along the homoclinic orbit, and therefore have been replaced by the constant ω_A. Solving this equation, we find the solution for the angle $\phi(t)$ along the homoclinic orbit as

$$\phi^h(t) = \omega_A t + \frac{4\sqrt{b}\alpha_2}{a}\tanh\sqrt{b}t, \tag{13}$$

where $\omega_A = \beta_2\delta - \lambda\Lambda_1 + 4\alpha_3 I$. We will be most interested in the change in phase, $\Delta\theta$, of the angle θ along the homoclinic orbit.

3.2. Dynamics on invariant plane

The dynamics on the manifold Π_0 can be characterized by one of two distinct assumptions. These assumptions involve the presence of a resonance on the manifold Π_0. Thus, we look at the dynamics of the system on the invariant plane, defined by

$$\Pi_0 = \{(x, y, I, \phi) | x = y = 0\},$$

which is invariant for any value of ε. The unperturbed flow on Π_0 is given by

$$\dot{I} = 0,$$
$$\dot{\phi} = \beta_2\delta - \lambda\Lambda_1 + 4\alpha_3 I = 4\alpha_3\left(I - \frac{\lambda\Lambda_1 - \beta_2\delta}{4\alpha_3}\right) = D_I H_0(\tilde{\mathbf{x}}_0(I), I). \tag{14}$$

For $I = I_0 \in (I_a, I_b)$, there is a resonance, i.e. $D_I H_0(\tilde{\mathbf{x}}_0(I), I) = 0$. In this case, the resonant value of $I = I_0$ corresponds to a circle of fixed points, denoted by $\mathscr{C}$. The rest of the manifold Π_0 contains periodic orbits, unless there is more than one resonance. In this case, we can define the quantity $\Delta\phi$, the phase change in the angle θ along the homoclinic

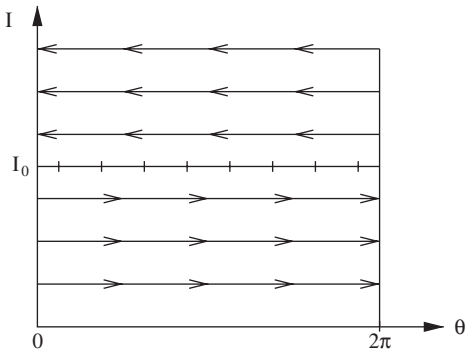

Fig. 2. Dynamics in the I–θ plane.

orbit at $I = I_0$, by

$$\Delta\phi = \phi^h(t = +\infty, I_0, \phi_0) - \phi^h(t = -\infty, I_0, \phi_0).$$

Every fixed point on the resonant circle $\mathscr{C}$ is connected to another point on that resonant circle by a single-pulse orbit. For our system, using Eq. (13), the phase shift in the angular coordinate ϕ on that orbit is given by

$$\Delta\phi = \phi(+\infty, I_0, \phi_0) - \phi(-\infty, I_0, \phi_0) = \frac{8\sqrt{b}\alpha_2}{a} = \frac{\alpha_2}{2\alpha_1}\sqrt{\beta_1\delta + 8\alpha_2 I_0}, \tag{15}$$

where a and b were defined in Eq. (12).

Thus, all orbits on this plane are circles or 1-tori. In particular, the orbit at $I_0 = (\lambda\Lambda_1 - \beta_2\delta)/(4\alpha_3)$ is a circle of fixed points, often denoted by $\mathscr{C}$. Of course, for a real physical system, we require that $I > 0$, so we must have that $I_0 = (\lambda\Lambda_1 - \beta_2\delta)/(4\alpha_3) > 0$ in order for $\mathscr{C}$ to exist. Since $\alpha_3 < 0$, and $\beta_2 > 0$ for the pipe we have the following conditions for the existence of $\mathscr{C}$:

$$\delta > \frac{\lambda\Lambda_1}{\beta_2}. \tag{16}$$

If this condition is satisfied, the frequency $\dot{\phi}$ vanishes at $I = I_0$. The fixed points at $I = I_0$ correspond to periodic solutions with the same frequency as the forcing frequency. The dynamics in the I–ϕ plane are illustrated in Fig. 2. In addition, we need to check that the twist condition holds, that is,

$$D_I^2 H_0(\Pi)|_{I=I_0} = 4\alpha_3 \neq 0 \tag{17}$$

holds at the resonant value of $I = I_0$. This condition assures that the frequency $\dot{\theta}$ has opposite signs on either side of the resonant value of I.

Next, we look at the eigenvalues of the system on the resonant circle $\mathscr{C}$. The linearization of the system on $\mathscr{C}$ is given by

$$\begin{bmatrix} 0 & \beta_1\delta + 8\alpha_2 I_0 & 0 & 0 \\ 1 & 0 & 0 & 0 \\ 0 & 0 & 0 & 4\alpha_3 \\ 0 & 0 & 0 & 0 \end{bmatrix}$$

with eigenvalues $0, 0, \pm\sqrt{(8\alpha_2 I_0 + \beta_1\delta)}$. Thus, the system has a pair of zero eigenvalues corresponding to directions in the plane Π_0. If $\delta > 8|\alpha_2|I_0/\beta_1$, then each point on the resonant circle is unstable, with real eigenvalues (one positive, one negative) in the directions transverse to the plane. This case is most important for our purposes, since it is the case in which a homoclinic orbit occurs in the x–y plane. If $\delta < 8|\alpha_2|I_0/\beta_1$, then each point on the resonant circle is stable, with pure imaginary eigenvalues in the directions transverse to the plane Π_0. We also note that for $\varepsilon > 0$, the manifold Π_0 remains invariant.

If we substitute in the resonant value of $I = I_0$ into the condition above for a homoclinic orbit to occur, we obtain a condition on δ and λ. This condition is given by using the fact that $\alpha_3\beta_1 - 2\alpha_2\beta_2 < 0$, see the discussion in McDonald

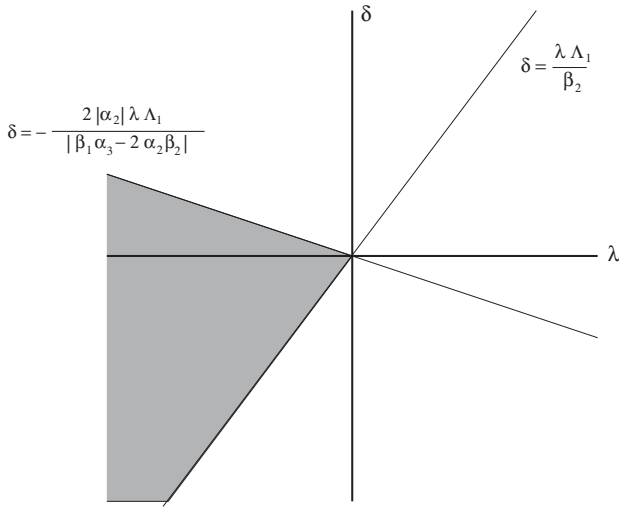

Fig. 3. Region where homoclinic orbit and resonant circle $\mathscr{C}$ both exist.

and Namachchivaya (2005)

$$\delta > -\frac{2|\alpha_2|\lambda\Lambda_1}{|\alpha_3\beta_1 - 2\alpha_2\beta_2|}.$$

Combining this condition with the conditions for a resonant circle to exist, (16), we obtain a region in the δ–λ plane where a resonant circle $\mathscr{C}$ exists in the invariant manifold, and an orbit homoclinic to that resonant circle exists in a plane parallel to the x–y plane. The global analysis in this paper will apply to these regions. Typical regions are shown for the pipe in Fig. 3.

3.3. Comparison to local analysis

Before continuing with the global analysis, we would like to compare the above results to the local results obtained in McDonald and Namachchivaya (2005), and compare the solutions and structures found in each analysis. Since slightly different scalings were used in these two analyses, the results will not correspond exactly. Also, the parameter δ was varied in the bifurcation diagrams in McDonald and Namachchivaya (2005), while δ is considered fixed in the phase portrait in Fig. 1. This difference makes it difficult to visualize the relationship between the local and global analyses.

For the local analysis, we found a first mode solution (in action-angle coordinates) which existed for $\delta > \zeta^2\delta_1^2/\beta_1$, and was given by

$$I_1 = \frac{\beta_1\delta}{64|\alpha_1|}(1 + \mathcal{O}(\zeta^2)).$$

In the global analysis, the analogue of these first mode solutions would be center fixed points $E_1^{\pm}$ that exist at $I = 0$ for $\delta > 0$. These fixed points are given in action-angle coordinates by

$$I_1 = \frac{\beta_1\delta}{64|\alpha_1|}.$$

Also, note that I_1 increases as δ increases, as was the case for the local analysis. The difference between the two cases lies in the fact that the damping has been scaled to be small in the global analysis, and hence does not enter into the unperturbed dynamics.

Next, we found a pair of second mode solutions in the local analysis. These solutions were given by

$$I_2 = \frac{(\lambda\Lambda_1 - \beta_2\delta) \pm \sqrt{\sigma_4^2 - \zeta^2\delta_2^2}}{4\alpha_3}.$$

The analogue for these solutions in the global analysis is the resonant circle of fixed points $\mathscr{C}$ that exists on the slow invariant manifold Π_0 at

$$I_2 = I_0 = \frac{\lambda\Lambda_1 - \beta_2\delta}{4\alpha_3}.$$

Since forcing and damping have been scaled to be small in the global analysis, the two solutions from the local analysis become one solution in the global analysis. Note that for the pipe, the resonant value I_0 (the circle of fixed points) increases as δ increases, while for the shaft, I_0 decreases as δ increases. This behavior corresponds to the super- and subcriticality of the second mode solutions for the pipe and shaft seen in the local analysis.

Finally, we found multi-mode solutions in the local analysis. These solutions connected the first mode solution to each of the two second mode solutions. These solutions bifurcated from the first and second mode solutions when those solutions became unstable due to the forcing. In the global analysis, since there is only one second mode solution, we can expect that there will be only one multi-mode solution, which we will denote by MM. A rough analogue of these multi-mode solutions are the two branches of fixed points $E_1^{\pm}(I_2)$ that connect the fixed points $E_1^{\pm}(I_2 = 0)$ to the invariant manifold Π_0. These branches intersect the invariant manifold Π_0 at $I_2 = \tilde{I}_2 = \beta_1\delta/(8|\alpha_2|)$. However, we must keep in mind that δ varies along MM. Thus, MM connects to Π_0 at $I_2 = \tilde{I}_2$ at a value of δ such that the circle of fixed points $\mathscr{C}$ is also located at $\tilde{I}_2$. Similarly, MM connects to $E_1^{\pm}(I_2 = 0)$ at a different value of δ. As mentioned earlier, it is difficult to compare the local and global pictures, since we consider δ fixed in the global analysis, but we vary δ in the local analysis. The local analysis will not be able to detect the more complicated global structures described later in this section.

4. Global dynamics near criticality

After obtaining detailed information on the nature of the unperturbed system, the next step is to examine the effects of small perturbations ($0 < \varepsilon \ll 1$) on the unperturbed dynamics. Now, we study the global bifurcations of simply supported damped pipe systems *near the critical velocity* u_c, when the fluid velocity is also pulsating. In Nagata and Namachchivaya (1998) for the autonomous case, the study of global solutions was made possible by assuming that the dissipation and the symmetry-breaking effects were small compared to the basic nonlinear effects. Global solutions were found using a Melnikov-type integrals to predict these global phenomena in a systematic manner. We extend this study to cover nonautonomous case in this paper.

The three methods we shall use can be called the *Melnikov method*, the *Šilnikov method*, and the *multi-pulse method*. The goal of each of these methods is to detect the presence of chaotic dynamics in the system studied. In the Melnikov method, we attempt to detect the transversal intersections of the stable and unstable manifolds of a hyperbolic fixed point. These intersections will lead to Smale horseshoes and chaotic dynamics. In the Šilnikov and multi-pulse methods, we attempt to detect the presence of single or multi-pulse orbits which are homoclinic to an equilibrium on the slow manifold. By applying Šilnikov's theorem, the presence of these orbits can be shown to lead to chaotic dynamics in the system. The existence of chaotic invariant sets near slow manifolds was first considered by Kovačič and Wiggins (1992). However, their formulation neglects one technical condition, which is filled in by Haller (1999), who also provides a review of much of the work in this area, and describes the multi-pulse method in some detail.

4.1. Non-resonant case

There is no resonance on the manifold Π_0, that is,

$$D_I H_0(\tilde{\mathbf{x}}_0(I), I) = 4\alpha_3\left(I - \frac{\lambda\Lambda_1 - \beta_2\delta}{4\alpha_3}\right) \neq 0$$

for all values of I in a region $(I_c, I_d) \subset (I_a, I_b)$ that does not contain the resonant value of $I = I_0$. In this case, the manifold Π_0 is a plane of periodic orbits (or 1-tori) with frequency $\Omega = D_I H_0(\tilde{x}_0(I), I)$, parameterized by the coordinate I. We first note that for small perturbations, the manifold Π_0 will persist, along with its stable and unstable manifolds. However, in general, the homoclinic manifold will break, and the stable or unstable manifolds may or may not intersect. The manifold Π_0 will perturb to a slow manifold Π_ε, given by

$$\Pi_\varepsilon = \{(\mathbf{x}, \phi, I) | \mathbf{x} = \tilde{\mathbf{x}}_0(I) + \varepsilon\tilde{\mathbf{x}}_1(I, \phi, \mu) + \mathscr{O}(\varepsilon^2), \tilde{I}_a < I < \tilde{I}_b, \phi \in (0, 2\pi)\}. \tag{18}$$

The perturbation $\tilde{\mathbf{x}}_1$ can be calculated from the equation

$$-(D_\theta\tilde{\mathbf{x}}_1)(D_I H_0) - JD_{\mathbf{x}}^2 H_0\tilde{\mathbf{x}}_1 = D_I\tilde{\mathbf{x}}_0 g^I - g^{\mathbf{x}}. \tag{19}$$

The dynamics on the manifold Π_0 also undergoes changes due to the perturbation. The equations on Π_ε, to leading order,

$$\dot{I} = \varepsilon g^I(\tilde{\mathbf{x}}_0(I), I, \theta, \mu; 0) + \mathcal{O}(\varepsilon^2),$$
$$\dot{\theta} = D_I H_0(\tilde{\mathbf{x}}_0(I), I) + \mathcal{O}(\varepsilon)$$

are identical to the equations on the unperturbed manifold Π_0. However, on the perturbed manifold, Π_ε, nearly all of the periodic orbits are destroyed, since $\dot{I} \neq 0$.

4.1.1. Melnikov method

If the system (14) does not possess a resonance, then we may apply the Melnikov method. To apply this method, we need to determine if any periodic orbits from Π_0 persist on the perturbed manifold. To this end, we can study the averaged system on Π_ε. Hence, we need to find a fixed point for the averaged system

$$\dot{\bar{I}} = \varepsilon G(I),$$

where

$$G(I) = \frac{1}{2\pi}\int_0^{2\pi} g^I(\tilde{\mathbf{x}}_0(I), I, \theta, \mu; 0)\,\mathrm{d}\theta.$$

For our system, this averaged system becomes

$$\dot{\bar{I}} = 2\zeta\delta_2 I + 4\zeta\phi_5 I^2,$$

which has fixed points given by $I = 0$ and $-\delta_2/2\phi_5$. However, $I = 0$ is only on the boundary of the homoclinic manifold, and the second fixed point is not stable. Therefore, the perturbed system does not possess any stable periodic orbits on Π_ε, and we cannot apply the Melnikov method here. Thus, the nonresonant system is not amenable to the global perturbation methods we have discussed. We therefore proceed to study the resonant case.

4.2. Resonant case

Again, we want to describe the effect of the perturbations on the resulting dynamics. Since the twist condition (17) holds, the frequency $\dot{\theta}$ has opposite signs on either side of the resonant value of I. For this case, the invariant manifold Π_0 persists. As in the nonresonance case, for the resonance case the manifold Π_0 will perturb to a slow manifold Π_ε, given by Eq. (18).

The dynamics on the manifold Π_0 undergoes a drastic change when the perturbation is added. To study the dynamics in a neighborhood of the resonance, we make a transformation that "blows up" the resonance-region. Hence, we make the standard coordinate transformation

$$I = I_0 + \sqrt{\varepsilon}\eta, \quad \phi = \phi,$$

and rescale time by $\tau = \sqrt{\varepsilon}t$. The new equations in this resonance region are given by

$$\eta' = 2\sigma_4 I_0 \sin 2\phi + (2\zeta\delta_2 I_0 + 4\zeta\phi_5 I_0^2)\phi + \sqrt{\varepsilon}G(\eta, \phi, \mu) + \mathcal{O}(\varepsilon),$$
$$\phi' = 4\alpha_3\eta + \sqrt{\varepsilon}F(\eta, \phi, \mu) + \mathcal{O}(\varepsilon),$$

where

$$G = (2\sigma_4 \sin 2\phi + 2\zeta\delta_2 + 8\zeta\phi_5 I_0)\eta, \quad F = \sigma_4 \cos 2\phi, \tag{20}$$

and where all functions are evaluated at $(\mathbf{x}, I, \phi, \mu; \varepsilon) = (\tilde{\mathbf{x}}_0(I_0), I_0, \phi, \mu; 0)$. One advantage of working in these local coordinates around the resonance is that the equations are Hamiltonian at leading order, i.e.

$$\eta' = 2\sigma_4 I_0 \sin 2\phi + (2\zeta\delta_2 I_0 + 4\zeta\phi_5 I_0^2)\phi = -D_\phi \mathscr{H},$$
$$\phi' = 4\alpha_3\eta = D_\eta \mathscr{H}, \tag{21}$$

where

$$\mathscr{H} = 2\alpha_3\eta^2 + \sigma_4 I_0 \cos 2\phi - (2\zeta\delta_2 I_0 + 4\zeta\phi_5 I_0^2)\phi.$$

We note that when damping is present, $\zeta \neq 0$, the system is only locally Hamiltonian, since the function $\mathscr{H}$ is not periodic in ϕ, and hence is not single valued for the leading order flow. Thus, to leading order, the dynamics near the resonance is locally Hamiltonian, even if damping is present in the system.

4.2.1. Šilnikov method

We want to determine the existence of Šilnikov orbits, that is, orbits which are homoclinic to the sink $\mathbf{p}_\varepsilon$. For such orbits to exist, we need to satisfy two conditions: a Melnikov-type condition and a phase condition.

We begin by studying the dynamics on the invariant manifold Π_0, which are described by Eqs. (21). Due to the π-symmetry of the equations, we need only look at the dynamics in $(-\pi/2, \pi/2)$. We can obtain two fixed points for the unperturbed system, given by

$$p_c = (\eta_c, \phi_c) = \left(0, \frac{1}{2}\sin^{-1}\frac{\zeta\delta_2 + 2\zeta\phi_5 I_0}{h\sigma_4}\right),$$
$$p_s = (\eta_s, \phi_s) = \left(0, \frac{\pi}{2} - \frac{1}{2}\sin^{-1}\frac{\zeta\delta_2 + 2\zeta\phi_5 I_0}{h\sigma_4}\right).$$

By examining, the stability of these two fixed points, we can determine that the first one represents a stable center-type fixed point, while the second represents an unstable saddle-type fixed point. When there is no damping in the system, the saddle points are at $\phi = \pm\pi/2$, and the center is at $\phi = 0$. The saddle fixed points will be connected to each other by a pair of heteroclinic orbits.

Next, we will examine the leading order dynamics in an annular region near the resonance defined by

$$\mathscr{A}_0 = \{(\eta, \phi) | -\eta_1 < \eta < \eta_1,\ \phi \in (0, 2\pi)\},$$

and η_1 is chosen to be large enough to contain the homoclinic orbit. When the $\mathscr{O}(\sqrt{\varepsilon})$ perturbation is included in the dynamics, the phase portrait of the integrable Hamiltonian unperturbed system will change. The perturbed equations will have the form

$$\eta' = -D_\phi \mathscr{H} + \sqrt{\varepsilon}G = P(\phi, \eta),$$
$$\phi' = D_\eta \mathscr{H} + \sqrt{\varepsilon}F = Q(\phi, \eta).$$

In particular, the saddle point will persist due to the persistence of hyperbolic fixed points under small perturbation. This new saddle point in the perturbed system will be denoted p_s^ε. The center point p_c may become either a source or a sink. To determine which, we will employ Bendixson's criterion. This criterion states that on a simply connected region $\mathscr{D}$, if the expression

$$T = \text{trace} = \frac{\partial P}{\partial h} + \frac{\partial Q}{\partial \phi}$$

is not identically zero, and does not change sign, then there are no closed orbits lying entirely in $\mathscr{D}$. Furthermore, if $T < 0$, then p_c will become a hyperbolic sink. The trace can be calculated from Eq. (20) and is given by $T = \sqrt{\varepsilon}(2\zeta\delta_2 + 8\zeta\phi_5 I_0)$. Since $\delta_2 < 0$ and $I_0 > 0$, the trace $T < 0$ if $\phi_5 < -\delta_2/4I_0$. This condition will hold if $\phi_5 < 0$. In this case, the center p_c will become a hyperbolic sink p_c^ε.

In addition, the homoclinic orbit of the unperturbed system with saddle p_s will be a good approximation to the basin of attraction of the sink p_c^ε (this homoclinic orbit will not generally persist under perturbation). We also denote the "nose" of this homoclinic orbit by ϕ_n. This nose can be determined by solving for ϕ_n in

$$\mathscr{H}(0, \phi_n) = \mathscr{H}(0, \phi_s).$$

To determine whether an orbit is homoclinic to the sink p_c^ε, we need to verify two conditions. First, we need to ensure that orbits in the unstable manifold of p_c^ε will return to the manifold Π_ε, i.e. $W^u(p_c^\varepsilon) \subset W^s(\Pi_\varepsilon)$. Thus, since we are trying to determine whether we have an intersection of a stable and an unstable manifold, we require the calculation of a Melnikov function. This Melnikov function calculates the distance between the two manifolds. A transverse zero of the Melnikov function indicates an intersection of the two manifolds.

4.2.2. Calculation of Melnikov function

The form of this Melnikov function is given by

$$M(I_0, \phi_c) = \int_{-\infty}^{\infty} \{\langle D_{\mathbf{x}} H_0, g^{\mathbf{x}}\rangle + (D_I H_0 \cdot g^I)\}\, \mathrm{d}t,$$

where the terms in the integrand are evaluated on the homoclinic orbit to the manifold Π_0 at the resonant value of $I = I_0$, i.e. $(\mathbf{x}^h(t, I_0), I_0, \phi^h(t, I_0, \phi_c))$. This integral can then be written as

$$M(I_0, \phi_c) = -\{H_1(t=\infty) - H_1(t=-\infty)\} + \int_{-\infty}^{\infty} \{\langle D_x H_0, f^{\mathbf{x}}\rangle + (D_I H_0 \cdot f^I)\}\,\mathrm{d}t, \tag{22}$$

where again, all terms in the integrand are calculated along the homoclinic orbit. First, we calculate $\Delta H_1 = H_1(t=\infty) - H_1(-\infty)$ for the subharmonic case

$$\Delta H_1 = H_1(t=\infty) - H_1(t=-\infty) = \sigma_4 I(\cos 2\phi(\infty) - \cos 2\phi(-\infty)).$$

But we note that $\phi(-\infty) = \phi_c$ and $\phi(\infty) = \phi_c + \Delta\phi$. Therefore, using $\phi_c = \frac{1}{2}\sin^{-1}(\zeta\delta_2 + 2\zeta\phi_5 I_0)/\sigma_4$ we have

$$\begin{aligned}\Delta H_1 &= \sigma_4 I_0(\cos[2(\phi_c + \Delta\phi)] - \cos 2\phi_c)\\ &= \sigma_4 I_0\left[\cos 2\Delta\phi\sqrt{1 - \left(\frac{\zeta\delta_2 + 2I_0\zeta\phi_5}{\sigma_4}\right)^2} - \sin 2\Delta\phi\,\frac{\zeta\delta_2 + 2I_0\zeta\phi_5}{\sigma_4}\right]\\ &= I_0\sqrt{\sigma_4^2 - (\zeta\delta_2 + 2I_0\phi_5)^2}\cos 2\Delta\phi - I_0(\zeta\delta_2 + 2I_0\zeta\phi_5)\sin 2\Delta\phi.\end{aligned}$$

The first integral in Eq. (22) can be evaluated using Green's theorem as

$$\begin{aligned}\int_{-\infty}^{\infty}\langle D_x H_0, f^{\mathbf{x}}\rangle\,\mathrm{d}t &= \int_A (2\zeta\delta_1 + 4\zeta\phi_1 I + 16\zeta\phi_2 y^2)\,\mathrm{d}x\,\mathrm{d}y\\ &= -\zeta(2\delta_1 + 4\phi_1 I_0)\frac{b\Delta\theta}{12\alpha_2(1+\lambda)} + (16\zeta\phi_2)\frac{b^2\Delta\theta}{30a\alpha_2(1+\lambda)},\end{aligned}$$

where A is the area of the homoclinic orbit in the x–y plane. The second term in the integral of (22) can be evaluated as

$$\int_{-\infty}^{\infty}(D_I H_0 \cdot f^I)\,\mathrm{d}t = \zeta(2\delta_2 I_0 + 4\phi_5 I^2)\Delta\theta - \frac{8\zeta\phi_6^r bI}{a}\Delta\theta. \tag{23}$$

Adding all of these terms together, we obtain an expression for the Melnikov function as

$$M(I_0, \phi_c) = -\sigma_4 I_0(\cos[2(\phi_c + \Delta\phi)] - \cos 2\phi_c) + \zeta K\Delta\theta,$$

where

$$K = -\frac{b(2\delta_1 + 4\phi_1 I_0)}{12\alpha_2(1+\lambda)} + \frac{16b^2\phi_2}{30a\alpha_2(1+\lambda)} + (2\delta_2 I_0 + 4\phi_5 I^2) - \frac{8\phi_6^r bI}{a}.$$

4.2.3. Calculation of phase condition

The second condition we need to check to see whether an orbit is homoclinic to the sink p_c^ε is the phase condition. Namely, we need to determine whether the orbit, when it returns to the manifold Π_ε, falls within the basin of attraction of the hyperbolic sink p_c^ε. As we said earlier, the homoclinic orbit of the unperturbed system on the manifold Π_0 is a good approximation to the basin of attraction of the hyperbolic sink. Thus, our phase condition can be expressed as

$$\phi_s < \phi(\infty) < \phi_n,$$

where $\phi(\infty) = \phi_c + \Delta\phi$. If the phase condition is satisfied, and the Melnikov function has transverse zeros as well, then we will have found an orbit homoclinic to the hyperbolic sink p_c^ε. Having satisfied the Melnikov condition and the phase condition, we now turn to Šilnikov's theorem. This version of Šilnikov's theorem is formulated in Deng (1993), and discussed in great detail in Haller (1999).

Theorem 4.1 (*Šilnikov, 1970*). *A four-dimensional system having a hyperbolic fixed point connected to itself by a homoclinic orbit is to be examined. The matrix associated with the fixed point is given by*

$$\begin{bmatrix} -\rho & -\omega & 0 & 0\\ \omega & -\rho & 0 & 0\\ 0 & 0 & -\lambda & 0\\ 0 & 0 & 0 & \nu\end{bmatrix}, \tag{24}$$

where $-\rho \pm i\omega$, $(\rho, \omega > 0)$ *are the eigenvalues of the vector field restricted to* $\mathscr{A}$, *where* $\mathscr{A} \subset \Pi$ *is the annular region containing the perturbed dynamics in* (η, θ), *and* $-\lambda$ *and* v $(\lambda, v > 0)$ *are the linearized growth rates transverse to* $\mathscr{A}$. *Assume the following*:

(i) $\rho < \lambda$ *and* $\rho < v$,
(ii) *the homoclinic orbit is isolated*,
(iii) *the homoclinic orbit is tangent to the eigenspace corresponding to the eigenvalues* $-\rho \pm i\omega$, *and*
(iv) *as time tends towards* $-\infty$, *points in the stable manifold of the homoclinic orbit should approach the strong stable manifold*.

If these four conditions are met, then a three-dimensional Poincaré map P defined near the homoclinic orbit has an invariant Cantor set, on which P is topologically conjugate to a sub-shift of finite type on infinitely many symbols. Thus, the perturbed flow will contain a countable set of Smale horseshoes.

For our system, the eigenvalues $-\rho \pm i\omega$ are $\mathcal{O}(\varepsilon)$, while the eigenvalues $-\lambda$ and v are $\mathcal{O}(1)$. Therefore, we only need to prove the existence of the homoclinic orbits, and show that $\lambda \neq v$ to be able to apply the theorem.

4.3. Multi-pulse orbits in forced-damped pipe

In this section, we will determine the existence of multi-pulse orbits for the system. Our goal is to detect orbits of the perturbed system which spend a lot of time near the slow manifold Π_ε, but make orbits with several pulses away from that slow manifold. In order to find multi-pulse orbits for the *perturbed* system, we will construct N-chains of single pulse orbits in the *unperturbed* system ($\varepsilon = 0$) to connect fixed points which are separated by a phase difference of $\Delta\theta$. These orbits represent fast transitions between resonances, or a quick excursion from a resonance, returning to the same solution, but with different phase. Now the N-pulse homoclinic orbits of the perturbed system will shadow the N-chains we have already described.

First, we want to determine if the energy functions are chain-independent. To do this, we calculate the inner product

$$\begin{aligned}\langle DH_0, g\rangle|_{I=I_0} = & -\zeta x(\delta_1 x + 2\phi_1 Ix + 4\phi_2 xy^2 + 4\phi_3^i Iy + 8\phi_4^i y^3) \\ & + \zeta(\beta_1\delta y + 32\alpha_1 y^3 + 8\alpha_2 Iy)(\delta_1 y + 2\phi_1 Iy + 4\phi_2 y^3) + \zeta(4\alpha_2 y^2)(2\delta_2 I + 4\phi_5 I^2 + 8\phi_6^r Iy^2).\end{aligned}$$

Note that this inner product does not depend on ϕ, and it is invariant under the transformation $(x, y) \to (-x, -y)$. These two facts allow us to conclude that the integral of this inner product will take the same value along any solution in either of the two symmetrically located homoclinic manifolds.

We will describe in an abbreviated form how to detect these orbits. We need to examine the dynamics of the system in two different regions:

(a) in a neighborhood of the invariant manifold $\mathscr{M}_\varepsilon$, where the orbits spend a majority of the time, and where we can use local estimates;
(b) away from the neighborhood of $\mathscr{M}_\varepsilon$, where the orbits spend very little time, and where the local coordinates are not defined. We will use the energy to track the orbits in this region.

First, examination of the dynamics of the system in a local neighborhood of the manifold $\mathscr{M}_\varepsilon$ requires many approximations and technical details, described in Haller (1999), but which we will not go into here.

We determine the energy difference function for the forced-damped case. The dissipative energy function is given by

$$\mathscr{H}_D = 2\alpha_3\eta^2 + \sigma_4 I_0 \cos 2\phi - (2\zeta\delta_2 I_0 + 4\zeta\phi_5 I_0^2)\phi.$$

with equations of motion given by

$$\begin{aligned}\dot{\eta} &= (2\zeta\delta_2 I_0 + 4\zeta\phi_5 I_0^2) + 2h\sigma_4 I_0 \sin 2\phi, \\ \dot{\theta} &= 4\alpha_3\eta.\end{aligned}$$

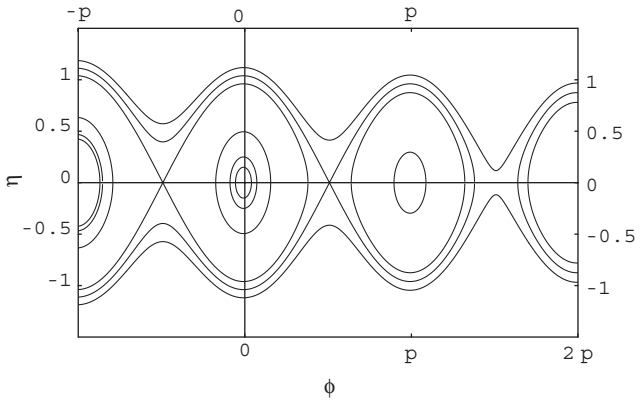

Fig. 4. Phase portrait for dissipative system, $\mathscr{H}_{\mathscr{D}}$.

The fixed points of this system are given by

$$(\eta_c, \phi_c) = \left(0, \frac{1}{2}\sin^{-1}\frac{\zeta\delta_2 + 2\zeta\phi_5 I_0}{\sigma_4}\right),$$
$$(\eta_s, \phi_s) = \left(0, \frac{\pi}{2} - \frac{1}{2}\sin^{-1}\frac{\zeta\delta_2 + 2\zeta\phi_5 I_0}{\sigma_4}\right).$$

The phase portrait for this local Hamiltonian is shown in Fig. 4 for the case $\zeta = 0.1$, $\delta_2 = -2$, $\phi_5 = 3$, $\sigma_4 = 2$, $\alpha_3 = -1$, and $I_0 = 0.5$.

Here, the analysis is restricted to cases for which $|(\zeta\delta_2 + 2\zeta\phi_5 I_0)/\sigma_4| \in (0, 1)$ in order to obtain physically meaningful results. We also notice that the saddles in the present case are connected to themselves by homoclinic connections as opposed to the purely Hamiltonian case where two saddles were connected by heteroclinic orbits. An annular region $\mathscr{A}$ can be defined as before in the neighborhood of the resonant structure such that it contains all the essential dynamics of the (η, ϕ) phase space for the dissipative case,

$$\mathscr{A} = \{(x, y, \eta, \phi) | x = 0, y = 0, -\eta_0 < \eta < \eta_0, \phi \in T^1\}, \tag{25}$$

where η_0 is large enough that $\mathscr{A}$ contains the entire homoclinic orbit.

The higher order (dissipative) perturbations in this case act to change the dynamical structure in a profound way. We can show that the trace of the linearization associated with the perturbed vector field is negative for $\zeta > 0$, and thus the hyperbolic saddles (ϕ_s) persist as saddles (ϕ_s^ε) and the elliptic centers (ϕ_c) become hyperbolic sinks (ϕ_c^ε). The periodic orbits surrounding the center (ϕ_c) are all destroyed and the homoclinic orbit connecting (ϕ_s) to itself is also broken, with its unstable manifold asymptotically approaching the hyperbolic sink (ϕ_c^ε).

4.3.1. Energy difference function

In order to show the existence of multi-pulse homoclinic orbits, it is important to obtain the expression for the energy difference function. The energy difference function is given by

$$\Delta^N \mathscr{H}(\phi) = \mathscr{H}(\phi + N\Delta\phi) - \mathscr{H}(\phi) - \sum_{l=1}^{N} \int_{-\infty}^{\infty} \langle DH_0, g\rangle|_{x_l(t)}\, \mathrm{d}t. \tag{26}$$

The first term in Eq. (26) was given earlier as

$$\mathscr{H}(\phi + N\Delta\phi) - \mathscr{H}(\theta) = \sigma_4 I_0[\cos 2(\phi + \Delta\phi) - \cos 2\phi]. \tag{27}$$

Applying Green's theorem, the integral in Eq. (26) evaluates to

$$\int_{-\infty}^{\infty} \langle DH_0, g\rangle|_{x_l(t)}\, \mathrm{d}t = \sigma \int_{A_l} \nabla_{x,y} \cdot g_{x,y}(x, y, I_0, \theta)\, \mathrm{d}x\, \mathrm{d}y + \int_{\partial A_l} g_I(x(\theta), y(\theta), I_0, \theta)\, \mathrm{d}\theta, \tag{28}$$

where A_l is the domain in the (x, y) plane which is encircled by the (x, y) component of the solution $x_l(t)$, and the constant $\sigma = -1$ ensures that we have the right orientation on the boundary of the region A_l. The first integrand is independent of l, so we can select the homoclinic orbit in the right half of the (x, y) plane for A_l. The first integral in (28)

can be simplified as

$$\sigma \int_{A_l} \nabla_{x,y} \cdot g_{x,y}(x, y, I_0, \theta)\, \mathrm{d}x\, \mathrm{d}y = \sigma \int_A \left[\frac{\mathrm{d}}{\mathrm{d}x} g^x(x, y, I_0, \phi) + \frac{\mathrm{d}}{\mathrm{d}y} g^y(x, y, I_0, \phi)\right] \mathrm{d}x\, \mathrm{d}y$$
$$= -\sigma(2\zeta\delta_1 + 4\zeta\phi_1 I)\frac{b\Delta\phi}{12\alpha_2} + 16\sigma\zeta\phi_2 \frac{b^2\Delta\phi}{30a\alpha_2}. \tag{29}$$

The third term in (28) is expressed as,

$$\int_{\partial A_l} g_I\, \mathrm{d}\phi = \left(2\zeta\delta_2 I + 4\zeta\phi_5 I^2 - \frac{8\zeta\phi_6^r bI}{a}\right)\Delta\phi. \tag{30}$$

Thus, combining the results of Eqs. (27), (29) and (30) our energy function can be written in the more compact form

$$\Delta^N \mathscr{H}(\phi) = -2\sigma_4 I_0 \sin(2\phi + N\Delta\phi)\sin N\Delta\phi + N\zeta K\Delta\phi,$$

where

$$K \stackrel{\text{def}}{=} \frac{-b\delta_1/6 + 8\phi_2 b^2/15a}{\alpha_2} + \left(-\frac{b\phi_1}{3\alpha_2} - 2\delta_2 + \frac{8\phi_6^r b}{a}\right) I_0 - 4\phi_5 I_0^2.$$

The zeros of $\Delta^n \mathscr{H}(\phi)$ are obtained by solving the expression

$$\sin(2\phi + N\Delta\phi) = \frac{\zeta NK\Delta\phi}{2\sigma_4 I_0 \sin N\Delta\phi}. \tag{31}$$

We define a dissipation factor $d = \zeta/\sigma_4$. Since the right-hand side of the previous equation must have magnitude less than 1, we have an upper bound on the value of the dissipation factor,

$$|d| < d_{\max} = \frac{2I_0}{NK\Delta\phi}|\sin N\Delta\phi|. \tag{32}$$

Thus, N-pulse orbits for a given pulse number N are not possible for all values of the dissipation ratio d, unlike the case of purely Hamiltonian perturbations. For small dissipation effects $d<1$, we have an upper bound on the maximum number of pulses

$$N < N_{\max} = \frac{2I_0}{|d|K\Delta\phi}. \tag{33}$$

It is apparent that the upper bound $N_{\max}$ is inversely proportional to the value of the dissipation factor. Thus, the infinite homoclinic tree breaks down into a finite tree even for very small values of the dissipation.

4.3.2. Zeros of the energy difference function

The transverse zeros of the dissipative energy difference function $\Delta^N \mathscr{H}(\phi)$ are given by the equation:

$$2\phi + N\Delta\phi = m\pi + (-1)^m \alpha, \tag{34}$$

where $m \in \mathbb{Z}$, and

$$\alpha = \sin^{-1}\frac{NdK\Delta\phi}{2I_0 \sin N\Delta\phi}. \tag{35}$$

If condition (32) is satisfied, then for any n satisfying $N\Delta\phi \neq l\pi$, $\forall l = 0, 1, 2, \ldots$, there are two transverse zeros of the dissipative energy difference function in the range $\phi \in [-\pi/2, \pi/2]$. Choosing the zeros in the range $\phi \in [-\pi/2, \pi/2]$, we obtain

$$\phi_{-1}^N = \frac{\pi}{2} - \left[\frac{N\Delta\phi}{2} + \frac{\alpha}{2}\right] \bmod \pi,$$
$$\phi_{-2}^N = \frac{\pi}{2} - \left[\frac{\pi}{2} + \frac{N\Delta\phi}{2} - \frac{\alpha}{2}\right] \bmod \pi. \tag{36}$$

We introduce the $N\Delta\phi$ translates of the two zeros given above

$$\phi_{+1}^N = [\phi_{+1}^N + N\Delta\phi] \bmod 2\pi,$$
$$\phi_{+2}^N = [\phi_{+2}^N + N\Delta\phi] \bmod 2\pi, \tag{37}$$

and define the two sets

$$\hat{Z}_-^N = \{(\eta,\phi) \in \mathscr{A} | \phi \in \{\phi_{-1}^N, \phi_{-2}^N\}\},$$
$$\hat{Z}_+^N = \{(\eta,\phi) \in \mathscr{A} | \phi \in \{\phi_{+1}^N, \phi_{+2}^N\}\}. \tag{38}$$

In a manner similar to the Hamiltonian case, we can consider a domain $E_1 \in \mathscr{A}$ enclosed inside the homoclinic orbit located in the interval $\phi \in [\phi^s, \phi^s + \pi]$. This domain is filled with periodic orbits which can be classified based on their pulse number. In this case, the energy sequence is defined as

$$h_0 = \mathscr{H}_g(0,\phi_s) = -I_0 h\sigma_4 \sqrt{1 - \frac{(\zeta\delta_2 + 2\zeta\phi_5 I_0)^2}{\sigma_4^2}} + I_0(\zeta\delta_2 + 2\zeta\phi_5 I_0)(2\phi_s - D),$$
$$h_n = \min[\mathscr{H}_g(0,\phi_{-1}^n), \mathscr{H}_g(0,\phi_{-2}^n)],$$
$$h_\infty = \mathscr{H}_g(0,\phi_c) = I_0 h\sigma_4 \sqrt{1 - \frac{(\zeta\delta_2 + 2\zeta\phi_5 I_0)^2}{\sigma_4^2}} + I_0(\zeta\delta_2 + 2\zeta\phi_5 I_0)(2\phi_c - D), \tag{39}$$

Table 1
Calculation of energy levels h_n and layer radii r_n in forced and damped system for $\Delta\phi = 1.2$

	ϕ_{-1}^n	$\mathscr{H}(0,\phi_{-1}^n)$	ϕ_{-2}^n	$\mathscr{H}(0,\phi_{-2}^n)$	h_n	Layer #	r_n
$n=1$	0.919	$-0.356\sigma_4 I_0$	-0.548	$0.511\sigma_4 I_0$	$0.511\sigma_4 I_0$	1	0.523
$n=2$	0.227	$0.876\sigma_4 I_0$	-1.056	$-0.409\sigma_4 I_0$	$0.876\sigma_4 I_0$	2	0.252
$n=3$	0.125	$0.956\sigma_4 I_0$	0.987	$-0.492\sigma_4 I_0$	$0.956\sigma_4 I_0$	3	0.150
$n=4$	-0.631	$0.366\sigma_4 I_0$	0.543	$0.410\sigma_4 I_0$	$0.410\sigma_4 I_0$	n/a	0.569
$n=5$	Condition (32) is not satisfied						
$n=6$	0.706	$0.087\sigma_4 I_0$	-0.052	$1.000\sigma_4 I_0$	$1.000\sigma_4 I_0$	6	0.027
$n=7$	0.060	$0.987\sigma_4 I_0$	-0.606	$0.412\sigma_4 I_0$	$0.987\sigma_4 I_0$	n/a	0.085
$n=8$	Condition (32) is not satisfied						
$n=9$	-0.149	$0.971\sigma_4 I_0$	0.344	$0.738\sigma_4 I_0$	$0.971\sigma_4 I_0$	n/a	0.124
$n=10$	Condition (32) is not satisfied						
$n=11$	Condition (32) is not satisfied						

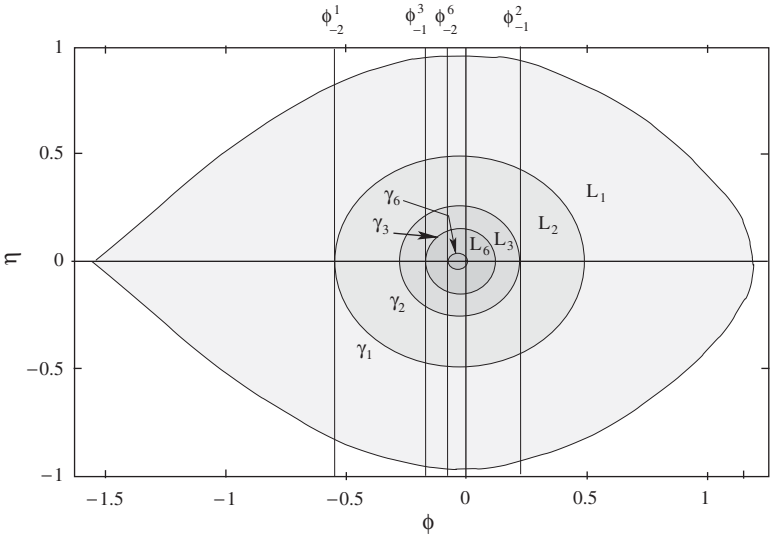

Fig. 5. Calculation of the layer sequence for $\Delta\phi = 1.2$.

such that $0<n<\infty$, and h_n gives the energy level associated with an orbit closer to the center. As for the Hamiltonian case, the energy increases as one moves towards the center fixed point. The open sets of internal orbits $\{\tilde{A}_n\}$, pulse sequence $\{N_k\}$, layer sequence $\{L_{N_k}\}$ are defined in the same manner as the nondissipative case. A sample calculation for these energy levels and layer radii is given in Table 1 for $\Delta\phi = 1.2$, $\zeta = 0.1$, $\delta_2 = -2$, $\phi_5 = 3$, $\alpha_3 = -1$, $I_0 = 0.5$ and $K = 1.6$. Note from condition (33) that $N<N_{\max} = 10.4$. Thus, we know a priori that there cannot be pulse numbers greater than $N = 10$ for this problem. We also note that for $n = \{5, 8, 10, 11, \ldots\}$, the limit on the damping, condition (32), is not satisfied. For these values of n then, the energy difference function does not have real zeros. Finally, we can see from the table that the system only has pulse numbers $N = \{1, 2, 3, 6\}$ at this set of parameters. We have also calculated the layer radii for the different layers. For these layers, the inner angular radii is given by

$$r_{N_k} = \min[|\phi_c - \phi_{-1}^{N_k}|, |\phi_c - \phi_{-2}^{N_k}|], \tag{40}$$

where $\phi_{-1}^{N_k}$ and $\phi_{-2}^{N_k}$ are given in Eq. (36). The zeros of the energy difference function and the layer sequence are also shown in Fig. 5 for the same parameter values. Note that the heteroclinic orbits for the Hamiltonian case are now homoclinic orbits, and the center fixed point is no longer at $\phi = 0$. The area inside the homoclinic orbit is split into five regions. In L_1, 1-pulse orbits are possible, in L_2, 2-pulse orbits are possible, in L_3, 3-pulse orbits are possible, and in L_6, 6-pulse orbits are possible. There is also a small region contained within L_6 in which no multi-pulse orbits are possible. It should be noted that all of these sequences are finite in the dissipative case. Thus, for any orbit $\gamma \in L_{N_k}$, we have the associated pulse number $N(\gamma) = N_k$.

The distribution of the pulse numbers and the layer radii are obtained by a recursive calculation, and is very sensitive to changes in system parameters. These distributions are shown in Figs. 6 and 7 for several values of the damping ζ, and

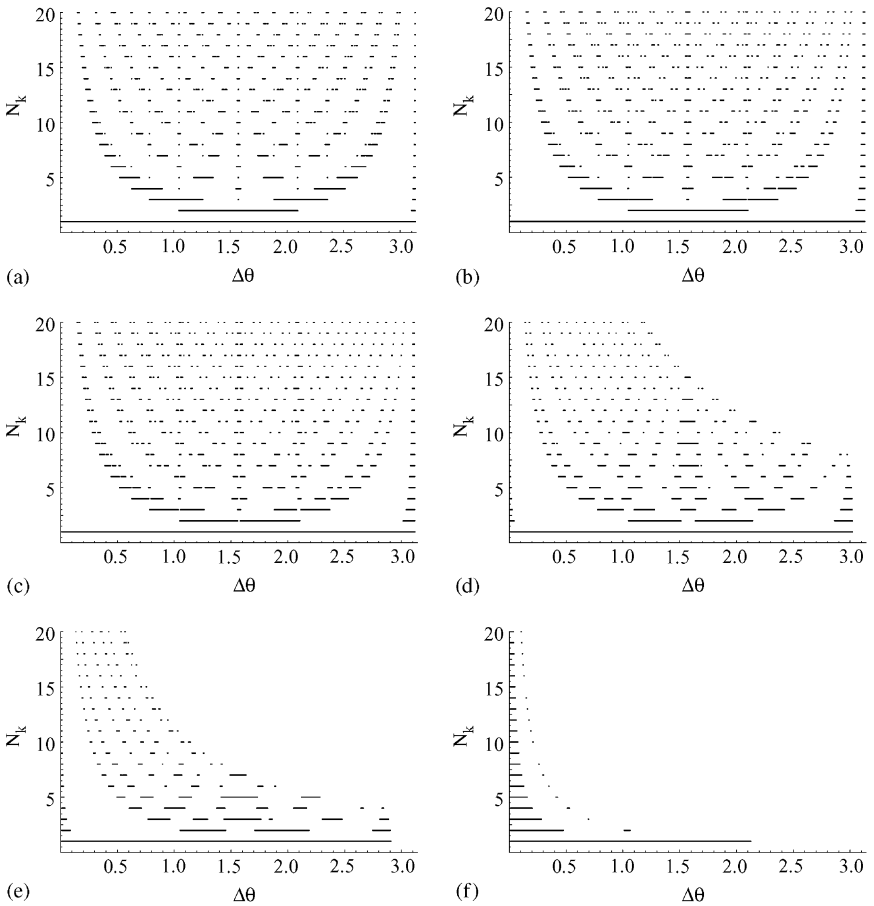

Fig. 6. Pulse numbers N_k as a function of the phase shift $\Delta\phi$ for several values of damping ζ: (a) $\zeta = 0.001$; (b) $\zeta = 0.005$; (c) $\zeta = 0.01$; (d) $\zeta = 0.05$; (e) $\zeta = 0.1$; (f) $\zeta = 0.5$.

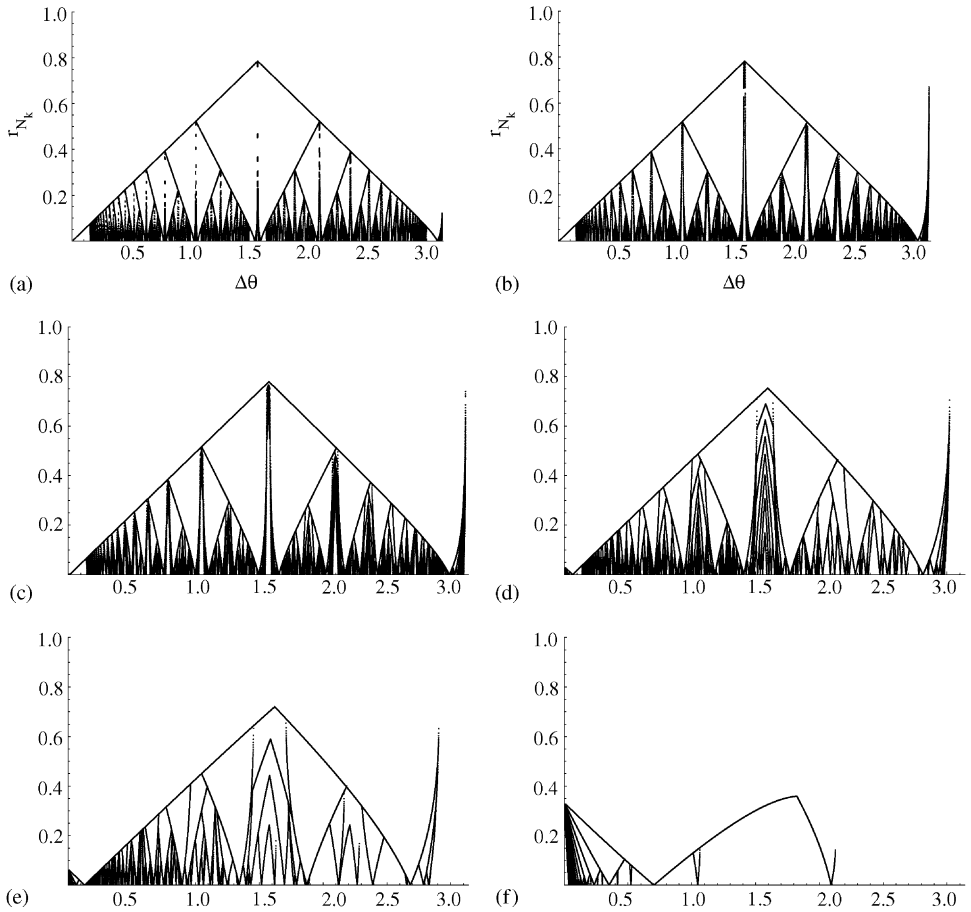

Fig. 7. Layer radii r_{N_k} as a function of the phase shift $\Delta\phi$ for several values of damping ζ: (a) $\zeta = 0.001$; (b) $\zeta = 0.005$; (c) $\zeta = 0.01$; (d) $\zeta = 0.05$; (e) $\zeta = 0.1$; (f) $\zeta = 0.5$.

for pulse numbers up to $N = 20$. Higher pulse numbers are possible, but as the pulse number increases, the range of $\Delta\phi$ in which that pulse number is found becomes smaller and smaller. Except for the damping, these plots use the same parameter values as in Table 1, namely $\delta_2 = -2$, $\phi_5 = 3$, $\alpha_3 = -1$, $I_0 = 0.5$ and $K = 1.6$. Note that as the damping increases, the distribution starts to break down further. In particular, the higher pulse orbits begin to disappear for higher values of $\Delta\phi$ as ζ is increased, while the number of multi-pulse orbits for small values of $\Delta\phi$ seems to increase. For $\zeta = 0.5$, multi-pulse orbits only exist for small values of $\Delta\phi$. The layer radii distribution, r_{N_k}, shows a similar breakdown as the damping is increased. The layer radii seem to increase near $\Delta\phi = \{\pi/4, \pi/2, 3\pi/4, \pi\}$ and other values of π/N. The pulse number is undefined at values of the phase shift given by $\Delta\phi = \pi/k$, where k is an integer. These values of $\Delta\phi$ correspond to resonant values of the phase shift, and the present methods will not work in this case. See Haller (1999) for more details on this case.

4.4. Detection of homoclinic orbits to saddle-sinks

In the Hamiltonian perturbation case, the existence of multi-pulse orbits implies that they are homoclinic to internal periodic orbits in the slow manifold Π_ε. However, in the dissipative case there are no such internal periodic orbits that lie on the slow manifold, and the center-type fixed point becomes a hyperbolic sink (or a saddle focus in the full four-dimensional phase space) due to the dissipative perturbations. Thus, in this case we look for multi-pulse orbits that are homoclinic to the saddle focus, i.e. Šilnikov-type multi-pulse orbits that are negatively and positively asymptotic to the saddle focus itself. The idea of N-pulse Šilnikov orbits is very similar to the single-pulse Šilnikov orbit. In an analogous

manner, the presence of N-pulse Šilnikov orbits leads to chaotic dynamics in the sense of Smale horseshoes. In order to determine the existence of such orbits, we apply Theorem 2.8.2 of Haller (1999).

First, we require the existence of a nondegenerate equilibria for $\mathscr{H}_g$. In the reduced (η, ϕ) phase space, this fixed point is given by

$$p^c = (\eta_c, \phi_c) = \left(0, \frac{1}{2}\sin^{-1}\frac{\zeta\delta_2 + 2\zeta\phi_5 I_0}{h\sigma_4}\right) = \left(0, \frac{1}{2}\sin^{-1} d(\delta_2 + 2\phi_5 I_0)\right). \tag{41}$$

Next, we need to compute the zeros of the dissipative energy difference function at the saddle center at $(0, 0, 0, \phi_c)$ in (x, y, η, ϕ) phase space. The zeros of $\Delta^N \mathscr{H}_g(\phi_c)$ are obtained by solving the equation

$$\Delta^N \mathscr{H}_g(\phi_c) = -2h\sigma_4 I_0 \sin(2\phi_c + N\Delta\phi)\sin N\Delta\phi + \zeta NK\Delta\phi = 0, \tag{42}$$

which yields

$$d(NK\Delta\phi - I_0(\delta_2 + 2\phi_5 I_0)\sin 2N\Delta\phi) = I_0\sqrt{1 - d^2(\delta_2 + 2\phi_5 I_0)^2}(1 - \cos 2N\Delta\phi). \tag{43}$$

Solving Eq. (43) for the dissipation parameter d, we obtain which yields

$$d = \frac{\zeta}{\sigma_4} = \frac{1 - \cos 2N\Delta\phi}{\sqrt{(\delta_2 + 2\phi_5 I_0)^2(1 - \cos 2N\Delta\phi)^2 + (NK\Delta\phi/I_0 - (\delta_2 + 2\phi_5 I_0)\sin 2N\Delta\phi)^2}}. \tag{44}$$

This result is only valid when the damping is nonzero, i.e.

$$\Delta\phi \neq \frac{m\pi}{N}, \quad m \in \mathbb{Z}. \tag{45}$$

We also need to satisfy the two nondegeneracy conditions

$$D_d \Delta^N \mathscr{H}_g(\phi_c) \neq 0 \quad \text{and} \quad D_{\phi_c} \Delta^N \mathscr{H}_g(\phi_c) \neq 0, \tag{46}$$

whenever Eqs. (44) and (45) are satisfied. The first condition in Eq. (46) can be rewritten as

$$D_d\left[\cos\left(\pi - \sin^{-1}\frac{d}{2} + 2N\Delta\phi_2\right) - \cos\left(\pi - \sin^{-1}\frac{d}{2}\right) + \frac{6nd}{1 + \sigma/\beta}\tan\frac{\Delta\phi_2}{2}\right] \neq 0. \tag{47}$$

After some simplification, we see that this condition is violated only if

$$\sqrt{1 - \frac{d^2}{4}}\left(\sin 2N\Delta\phi_2 - \frac{12N\tan\Delta\phi_2/2}{1 + \sigma/\beta}\right) = \frac{d}{2}(\cos 2N\Delta\phi_2 - 1). \tag{48}$$

Obviously, conditions (43) and (48) cannot both be satisfied if Eq. (45) is also satisfied. The second nondegeneracy condition in Eq. (46) is satisfied by the existence of transversal zeros of $\Delta^N \hat{\mathscr{H}}_D$, and is thus satisfied by inequality (32).

Finally, we need to insure that the landing point of any N-pulse orbit taking off from a slow sink lies in the domain of attraction of one of the sinks. We first define a point which is in the interval $[0, \pi]$, and is $k\pi$ apart from the approximate landing point, $\phi_c + N\Delta\phi$. We denote this point by

$$\phi_*^N = \phi_s + [\phi_c + N\Delta\phi - \phi_s] \bmod \pi, \tag{49}$$

where we recall that

$$\phi^c = \frac{\pi}{2} - \frac{1}{2}\sin^{-1}\frac{d}{2}, \quad \phi^s = \frac{1}{2}\sin^{-1}\frac{d}{2}. \tag{50}$$

If $\phi_*^N < \phi^s$, then we redefine ϕ_*^N by adding π to its value. Our goal here is to find $k\pi$-translate of the landing point which is closest (on the right-hand side) to the saddle point ϕ^c in our domain of interest $(0, \pi)$. This point is denoted by ϕ_*^N. Due to the symmetry of the phase portrait $\phi \to \phi + \pi$, if the energy of this point, ϕ_*^N, is greater than the energy of the saddle point, i.e.

$$\mathscr{H}_D(0, \phi_*^N) < \mathscr{H}_D(0, \phi^s), \tag{51}$$

then for $\varepsilon > 0$ small enough, the landing point $\phi + N\Delta\phi^c$ will be in the domain of attraction of one of the sinks. This energy condition (51) is evaluated as

$$\cos 2\phi_*^N - \cos 2\phi^s < d(\phi^s - \phi_*^N). \tag{52}$$

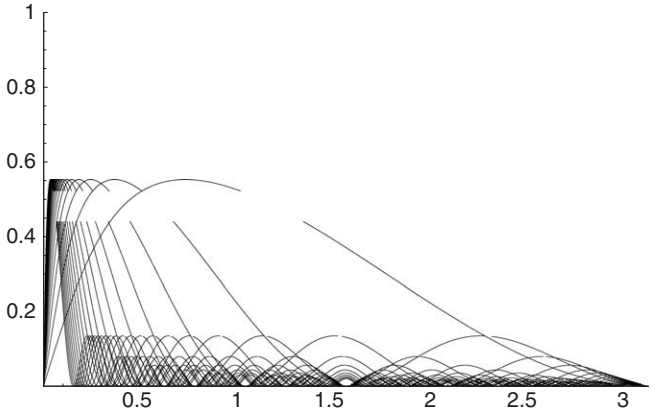

Fig. 8. Parameter set for which multi-pulse Šilnikov orbits may exist for pulse numbers $N<20$.

The parameter set for which multi-pulse Šilnikov orbits may exist is shown in Fig. 8 for pulse numbers $N\leqslant 20$, and $\zeta = 0.1$, $\delta_2 = -2$, $\phi_5 = 3$, $\alpha_3 = -1$, $I_0 = 0.5$ and $K = 1.6$, i.e. the same conditions that were used earlier. This figure was plotted by first plotting (44) for the pulse numbers up to $N = 20$, and then removing the parts of the curve for which the phase condition was violated.

5. Conclusions

We can now summarize the results of the global bifurcation analysis. In this paper, we detected the presence of orbits which are homoclinic to certain invariant sets on the slow manifold Π_ε for the resonant case. In the dissipative case, we were able to identify conditions under which a generalized Šilnikov orbit would exist. Under such conditions, the system would undergo chaotic dynamics in the sense of Smale horseshoes.

In studying a real physical system, one should be mindful of the sensitivity of these multi-pulse orbits to changes in system parameters. Since uncertainties always exist in real engineering systems, it would be unwise to use the results of this paper to attempt to precisely predict where multi-pulse orbits with a certain number of pulses might occur. For example, one should not look at Fig. 6 and attempt to conclude that, say, 10-pulse orbits exist for a certain set of system parameters. The important conclusion to draw from this paper is that in certain parameter regions, several families of multi-pulse orbits, with different numbers of pulses, are likely to occur, and that this pulse distribution is likely to change drastically with small changes in system parameters. In addition, the multi-pulse orbits homoclinic to the saddle focus points p_c^ε only exist on co-dimension one sets in the parameter space. However, the horseshoes that they generate are structurally stable, and thus the system will admit Smale horseshoes in its dynamics in an open neighborhood of the plot given in Fig. 8.

Next, we would like discuss a synthesis of the local and global bifurcation results. Unfortunately, such an integration of these two sets of results is not entirely possible, since different assumptions and scalings were made in each of these analyses. For example, in the local bifurcation analysis (McDonald and Namachchivaya, 2005), the presence of the subharmonic forcing allowed for the creation of second mode solutions, in addition to the first mode solutions created by the symmetry breaking. The first mode solutions have an analogue in the global analysis for $I_2 = 0$, as the center fixed points that bifurcate from the trivial solution and are surrounded by the homoclinic orbits in the x–y plane. It is more difficult to find an analogue in the global analysis to the second mode solutions that bifurcate from the trivial solution. In the global analysis, the damping and forcing terms are regarded as perturbations, and scaled to $\mathcal{O}(\varepsilon)$. We then study the dynamics of the unperturbed system, for which $\dot{I} = 0$ identically. If we scale the damping and forcing to $\mathcal{O}(\varepsilon)$ in the second mode solutions found in the local analysis in McDonald and Namachchivaya (2005), then these two second mode solutions reduce to one solution, which is identical to the resonant value of I_2 given in Section 4. Thus, the resonant value of I_2 corresponds roughly to the second mode solutions in the local analysis. The multi-mode solutions from the local analysis then correspond to a transfer of energy from the second mode solutions to the first mode solutions, and vice versa. Again, if damping and forcing are scaled to $\mathcal{O}(\varepsilon)$, then the existence criterion of these multi-mode solutions is equivalent to the conditions in the global analysis that a homoclinic orbit exists (i.e. the plane Π_0 is unstable), and a resonance exists on Π_0. Thus, both the local and global analysis gives essentially the same information

about where energy transfer may occur between the two modes. The advantage of the global analysis is that it allows us to study how the energy is transferred between the modes, which in this case may be through the presence of chaotic dynamics near the multi-pulse orbits.

Acknowledgements

The first author would like to acknowledge the support of National Science Foundation under Grant number CMS 03-01412. Any opinions, findings, and conclusions or recommendations expressed in this paper are those of the authors and do not necessarily reflect the views of the National Science Foundation.

References

Deng, B., 1993. On Šilnikov's homoclinic saddle-focus theorem. Journal of Differential Equations 102, 305–329.

Feng, Z., Sethna, P.R., 1993. Global bifurcations in the motion of parametrically excited thin plates. Nonlinear Dynamics 4, 398–408.

Guckenheimer, J., Holmes, P., 1983. Nonlinear Oscillations, Dynamical Systems, and Bifurcations of Vector Fields. Springer, New York.

Haller, G., 1998. Multi-dimensional homoclinic jumping and the discretized NLS equation. Communications in Mathematical Physics 193, 1–46.

Haller, G., 1999. Chaos Near Resonance. Springer, New York.

Haller, G., Wiggins, S., 1995. Multi-pulse jumping orbits and homoclinic trees in a modal truncation of the damped-forced nonlinear Schrödinger equation. Physica D 85, 311–347.

Kovačič, G., Wettergren, T.A., 1996. Homoclinic orbits in the dynamics of resonantly driven coupled pendula. Zeitschrrift fuer Angewandte Mathematik and Physik 47, 221–264.

Kovačič, G., Wiggins, S., 1992. Orbits homoclinic to resonances, with an application to chaos in a model of the forced and damped Sine–Gordon equation. Physica D 57, 185–225.

Malhotra, N., Namachchivaya, N. Sri., 1995. Global bifurcations in externally excited two-degrees-of-freedom nonlinear systems. Nonlinear Dynamics 8, 85–109.

McDonald, R., Namachchivaya, N. Sri., 2005. Pipes conveying pulsating fluid near a 0 : 1 resonance: local bifurcations. Journal of Fluids and Structures.

McDonald, R.J., Murdouck, J.A., Namachchivaya, N. Sri., 1999. Normal forms for nonlinear Hamiltonian systems with weak periodic perturbations. Journal of Dynamics and Stability of Systems 14, 187–211.

Melnikov, M.H., 1963. On the stability of the center for time periodic perturbations. Transactions of the Moscow Mathematical Society 12, 1–57.

Nagata, W., Namachchivaya, N. Sri., 1998. Bifurcations in gyroscopic systems with an application to rotating shafts. Proceedings of the Royal Society: Series A 454, 543–585.

Šilnikov, L.P., 1965. A case of the existence of a countable number of periodic motions. Soviet Mathematics Doklady 6, 163–166.

Šilnikov, L.P., 1970. A contribution to the problem of the structure of an extended neighborhood of a rough equilibrium state of saddle-focus type. Mathematics USSR Sbornik 10, 91–102.

Tien, W.M., Namachchivaya, N. Sri., Bajaj, A.K., 1994a. Nonlinear dynamics of a shallow arch under periodic excitation, Part I: 1:2 internal resonance. International Journal of Nonlinear Mechanics 29, 349–366.

Tien, W.M., Namachchivaya, N. Sri., Malhotra, N., 1994b. Nonlinear dynamics of a shallow arch under periodic excitation, Part II: 1:1 internal resonance. International Journal of Nonlinear Mechanics 29, 367–386.

Wiggins, S., 1988. Global Bifurcations and Chaos. Springer, New York.

Further reading

Malhotra, N., Namachchivaya, N. Sri., McDonald, R.J., 2002. Single and multi-pulse orbits in the motion of flexible spinning discs. Journal of Nonlinear Science 12, 1–26.

Namachchivaya, N. Sri., Tien, W.M., 1989. Bifurcation behavior of nonlinear pipes conveying pulsating flow. Journal of Fluids and Structures 3, 609–629.